Changing Snow Regime Classifications across the Contiguous United States

Molly E. Tedesche[1, 2], Travis A. Dahl[1], and Jeremy J. Giovando[2]

[1] Coastal and Hydraulics Laboratory, US Army Corps Engineer Research and Development Center, Vicksburg, MS, USA.

[2] Cold Regions Research and Engineering Laboratory, US Army Corps Engineer Research and Development Center, Hanover, NH, USA.

Corresponding author: Molly E. Tedesche (metedesche@alaska.edu)

Key Points:

- Average snow cover duration generally became shorter in each decade over the 40-year period from 1980 to 2020, with the rate of decline increasing with elevation.
- CONUS-wide areal extents of snow dominated regions decreased from the 1980s through the 1990s and 2000s, while those of rain dominated increased.
- Previously snow dominated areas have shifted to the transitional classification over the 40-year period, with the boundary lines moving up in latitude.

Abstract

Much of the world's water resource infrastructure was designed for specific regional snowmelt regimes under the assumption of a stable climate. However, as climate continues to change, this infrastructure is experiencing rapid regime shifts that test design limits. These changing snowmelt cycles are responsible for extreme hydrologic events occurring across the Contiguous United States (CONUS), such as river flooding from rain-on-snow, which puts infrastructure and communities at risk. Our study uses a new spatial snow regime classification system to track climate driven changes in snow hydrology across CONUS over 40 years (1981 – 2020). Using cloud-based computing and reanalysis data, regime classes are calculated annually, with changes evaluated across decadal and 30-year normal time scales. The snow regime classification designates areas across CONUS as: (1) rain dominated (RD), (2) snow dominated (SD), (3) transitional (R/S), or (4) perennial snow (PS). Classifications are thresholded using a ratio of maximum snow water equivalent (SWE) over accumulated cool-season precipitation, with a comparison of two approaches for selecting maximum SWE. Results indicate that average snow cover duration generally became shorter in each decade over our evaluation period, with rates of decline increasing at higher elevations. Anomalies in SD spatial extents, compared to the 30-year normal, decreased over the first three decades, while anomalies in RD extents increased. Also, previously SD areas have shifted to R/S, with boundary lines moving up in latitude. As water managers adapt to a changing climate, geospatial classification, such as this snow regime approach, may be a critical tool.

Plain Language Summary

As climate change continues, the United States is experiencing rapid shifts in snowmelt cycles for which water resource infrastructure across the country was not designed. Changes in snowmelt patterns can cause extreme events, such as river flooding from rain-on-snow (RoS). Our study uses climate model data to create new classification maps that show changes in snow across the US for the last 40 years (1981 – 2020). These classes include: (1) rain dominated (RD), (2) snow dominated (SD), (3) transitional (R/S), and (4) perennial snow (PS). Over the study period, our results show that snow covers the ground for shorter portions of each year, especially in mountainous areas. We also find that previously snow dominated areas are becoming a mixture of both rainfall and snowfall during the winter months. These types of changes can increase the likelihood of RoS flood events, putting infrastructure and communities at risk. This new classification system could help those who must manage such risks.

1 Introduction

As the global climate continues to change, weather station records from the late 20th century, and into the 21st, indicate that timing (Pan et al., 2021; Vano et al., 2015), duration (Knowles, 2015; Stone et al., 2002; Svoma, 2011), and quantities (Kunkel et al., 2016) of snowfall and snowmelt are shifting rapidly. Climate model simulations also project continued changes in snow hydrology across the planet (Schnorbus et al., 2014; Vormoor et al., 2015), with accelerated rates of change moving into the future (Lader et al., 2020). Much of the world's water resource infrastructure was designed for specific snowmelt regimes under the assumption of a stable climate. However, changing snowmelt cycles have recently been linked to extreme hydrologic and climatic events occurring across the Contiguous United States (CONUS) and globally. Some of

these events include river flooding from rain-on-snow (RoS) (Musselman et al., 2018), as well as extreme wildfires (Giovando & Niemann, 2022; Goss et al., 2020), all of which put infrastructure and local communities at risk. Numerous studies have provided ample evidence of long-term declines in snow cover across CONUS during the last forty years (1980 to 2020) (Brown, 2000; Groisman et al., 2004; Nolin et al., 2021). Long-term declines in snow cover duration (SCD) and snowfall quantities in CONUS have been punctuated with shorter term inter-annual increases (Kunkel et al., 2009), as well as localized increases in snowfall frequency in certain regions of CONUS (Kluver & Leathers, 2015). Nonetheless, the overall trend paints a picture of a declining snowpack and associated increases in extreme weather events that are already occurring throughout CONUS.

Extreme weather, such as flooding from RoS events, may be increasing in frequency in some regions of CONUS due to climate-driven changes in snow hydrologic regimes (Musselman et al., 2018), but parsing out trends in frequency of RoS events is anything but straight forward. RoS flooding occurs when the internal temperature of the snowpack is nearly isothermal (0^{o} C). Additional energy inputs cause a snow crystal phase change to liquid water, resulting in snowmelt. Typically, snowmelt is initiated in the spring, as energy inputs gradually increase from additional solar radiation from the winter through the summer solstice. Wintertime rainfall can also provide similar additional energy inputs to the snowpack. Snow cover variables, such as crystal structure and depth, can have a modulating effect on RoS flood volumes and timing (Wever et al., 2014), as can a colder snowpack (Würzer et al., 2017). However, if an extreme rainfall event occurs over an isothermal snowpack, combined snowmelt and rainfall volumes can reach the soil surface, resulting in substantial runoff to streams and rivers. Previous studies have attempted to partition the contributions to RoS runoff volumes between snowmelt versus rainfall using both empirical observations (Rücker et al., 2019) and physically based models (Wayand et al., 2015). These studies showed snowmelt contributions to streamflow ranging from about 7% to 30% during RoS events, indicating flood forecasting should prioritize rainfall prediction, but not neglect snowmelt contributions (Rücker et al., 2019; Wayand et al., 2015).

The complexity of RoS physical processes makes it difficult to forecast future RoS-induced flooding (Li et al., 2019; Musselman et al., 2018), future frequency of RoS events across CONUS (McCabe et al., 2007), or to determine trends in historic RoS events using past weather station records (Li et al., 2019; Wachowicz et al., 2020). Therefore, a continuing need exists to develop additional approaches to pinpoint regions where RoS flooding could occur and to determine these events' dependency on topographic variables such as latitude and elevation (López-Moreno et al., 2021; McCabe et al., 2007), as well as dependency on climate-driven changes in air temperature (McCabe et al., 2007), snowpack properties (Pradhanang et al., 2013; Singh et al., 1997) and precipitation phase shifts (Heggli et al., 2022; Marks et al., 2013). Previous studies have also used remote sensing and snowmelt modeling techniques (Hamill et al., 2021) to identify (Dolant et al., 2016; Grenfell & Putkonen, 2008; Ocampo Melgar & Meza, 2020; Pan et al., 2018) and simulate future occurrences (Marks et al., 1998, 2001; Mazurkiewicz et al., 2008; Qi et al., 2017; Würzer et al., 2016) of RoS events, respectively. In this study, we create a snow regime classification system, which could be used to ascertain vulnerability to RoS events for specific localized regions across CONUS, among other potential resource management applications.

Our snow regime classification system designates areas across CONUS as: (1) rain dominated (RD), (2) snow dominated (SD), (3) transitional (R/S), or (4) perennial snow (PS). The first three of these classes (RD, SD, and R/S) were developed in previous studies using the ratio

of maximum snow water equivalent (SWE) to cumulative cool season (October through March) precipitation (Barnett et al., 2005; Mantua et al., 2010; Tohver et al., 2014). Warmer RD systems produce runoff coincident with seasonal precipitation, while colder SD regions store a significant fraction of cool season precipitation as snowpack, resulting in snowmelt induced spring and summer runoff (Tohver et al., 2014). R/S systems typically have two annual runoff peaks, one in fall/early winter from rainfall and one in spring/summer from rainfall plus snowmelt (Tohver et al., 2014). In 2008, Barnett et al. showed that these ratios have declined in the western CONUS due to anthropogenically influenced climate warming. Meanwhile, in 2007, Hamlet and Lettenmaier characterized the three classes by air temperature for watersheds in the Pacific Northwest (PNW) of CONUS. Regions classified as R/S are of particular concern, as they are typically most vulnerable to RoS flooding, due to earlier and/or ephemeral snow melt, coupled with an increased proportion of cool season precipitation occurring as rain rather than snow (Tohver et al., 2014).

Some studies have utilized relationships between snow variables, precipitation, and air temperature to simulate stream flow into the Columbia River basin (Elsner et al., 2010), to delineate seasonal versus transient snow in mountainous regions of the PNW (Jefferson, 2011), and to map the rain-snow transition zone across the western CONUS (Klos et al., 2014). A ratio similar to the one used in our study, of winter-total snowfall water equivalent to winter-total precipitation (November through March) was employed by Knowles et al. (2006) to show that fractions of precipitation falling as snow declined, while those of rain increased in western North America. While not utilizing the SWE to precipitation ratio directly, several other studies have characterized streamflow regimes based on source categories such as rainfall, snowmelt, and high elevation glacier melt or mixed in Alaska (Curran & Biles, 2021); as well as rainfall, snowmelt, or mixed along the Colorado Front Range in the Rocky Mountains (Kampf & Lefsky, 2016).

Other research takes different approaches to creating snow classes that we do not directly employ here, yet their utility is worth noting, such as global snow persistence zones (intermittent, seasonal, permanent) (Hammond et al., 2018; Harrison et al., 2021; Saavedra et al., 2017); ecological region snow cover classes (tundra, taiga, alpine, maritime, prairie, ephemeral) (Sturm et al., 1995); topographically based snow categories (persistent, transitional, intermittent, seasonal) (Kampf & Richer, 2014; Moore et al., 2015; Richer et al., 2013); snow regimes based on temporal snowpack metrics such as accumulation and melt dates (maritime, intermountain, continental) (Trujillo & Molotch, 2014); and snow cover classification using a rain-snow threshold temperature (Nolin & Daly, 2006).

The purpose of this research is to create a Snow Regime Classification system for CONUS in order to detect climate-driven changes in regional snowmelt cycles. An additional goal is to provide these classifications as a practical, accessible geospatial tool for use by water resource managers, land managers, and other researchers and stakeholders. In order to detect climate-driven changes in snowmelt regimes across CONUS, the results of our study are quantified and evaluated as average decadal and 30-year normal spatial summary maps.

To meet the purpose and goal of the research, ***three objectives*** are addressed in this study: ***(1)*** Develop a dataset-agnostic evaluation framework for the gridded snow water equivalent (SWE) reanalysis dataset; ***(2)*** develop the Snow Regime Classification system using gridded climate data, spatial math, and thresholding of numerical results into discrete classes; and ***(3)*** compare two data-driven approaches to generating the Snow Regime Classifications across CONUS.

2 Data Sources

The primary datasets used in this study to create the Snow Regime Classification system for CONUS are daily gridded climate reanalysis data, including precipitation and snow water equivalent (SWE). The daily 4km gridded precipitation data is taken from the Parameter-elevation Regressions on Independent Slope Model (PRISM) and covers the spatial extent of CONUS (Daly et al., 2021, PRISM, 2022). As explained further below in the methods section, analyses for this study were conducted using Google Earth Engine (GEE), a cloud-computing platform for planetary scale geospatial analysis (Gorelick et al., 2017). Therefore, all PRISM data were accessed and processed directly from within the GEE application program interface (API) environment (*developers.google.com/earth-engine/datasets/catalog/OREGONSTATE_PRISM_AN81d*). PRISM image properties via GEE include a ***status*** property, which labels data generated within 30 days of observation as "early, data generated within 1 to 6 months of observation as "provisional", and data older than 6 months as "permanent". All PRISM data used in our study are considered ***permanent.*** The main variable of interest taken from PRISM is gridded precipitation, which is used in the principal calculations for this study. However, gridded air temperature from PRISM was subsequently used to investigate some results.

The PRISM dataset is derived from calculations involving a climate elevation-regression in each grid cell of a digital elevation model (DEM), where weather station data input into the regression are assigned weights based on physical variables such as geographic coordinates, elevation, coastal proximity, topographic orientation, vertical atmospheric layer, topographic position, and orographic effectiveness (Daly et al., 2008). In 2017, Strachan and Daly tested the daily PRISM air temperature data over semiarid mountainous terrain by comparing model estimates with in-situ data at 16 sites within the Walker River Basin in the western US, a watershed on the climate transition zone between the Sierra Nevada and Great Basin Desert. They found that on-the-ground temperature conditions were more heterogeneous than the interpolated PRISM models could predict (Strachan & Daly, 2017). However, also in 2017, Daly et al. were able to ground truth PRISM precipitation grid data with a 69 station rain gauge network in western North Carolina, USA that was maintained from 1951 to 1958. In their estimations of uncertainty, they found the PRISM national grids matched closely (to within 5%) of that rain gauge network in the southern Appalachians (Daly et al., 2017).

The SWE dataset used in this study is part of the Daily 4 km Gridded SWE and Snow Depth from Assimilated In-Situ and Modeled Data over the Conterminous US, Version 1 (*nsidc.org/data/nsidc-0719*). These gridded SWE data were developed at the University of Arizona (Broxton et al., 2016) and are hereafter referenced as the UA SWE data in our study. In order to create the modeled UA dataset, Broxton et al. (2016) used observational data from the United States (US) Natural Resources Conservation Service (NRCS) automated Snow Telemetry (SNOTEL) weather stations in the western US, as well as from manual measurements across CONUS via the US National Oceanic and Atmospheric Administration (NOAA) National Weather Service (NWS) Cooperative Observer network. They created the SWE and snow depth gridded dataset for CONUS via the spatial interpolation of empirical snow cover variables, and constrained it by daily PRISM precipitation totals. The UA SWE estimates are also computed on the same 4km resolution grid as the PRISM dataset. In 2018, Dawson et al. demonstrated that snow cover extents derived from the UA SWE dataset had an overall close agreement with three high resolution satellite derived snow cover extent products, including GlobSnow SWE (Takala et al., 2011). Additionally, a very high correlation of 0.98, with 30% relative mean absolute deviation, was

found between the UA SWE dataset and snow depths from the Airborne Snow Observatory (ASO) Light Detection and Ranging (LiDAR) dataset (Dawson et al., 2018; Zeng et al., 2018).

To validate a small number of gridded UA SWE values, observational snow cover data from on-the-ground weather stations were utilized. These stations are spread across CONUS in several key regions. Those located in the Midwest and Eastern CONUS are part of the Weather Bureau Army Navy (WBAN) network, consisting of federal airports where weather data are collected. WBAN stations report snow depth in inches and SWE by tenths of inches and data are transmitted in a METAR (Meteorological Terminal Aviation Routine Weather Report) along with other observations (NOAA, 2019). Eastern CONUS observational snow cover data was previously compiled by Engel at al. (2022) and readily available. For the UA SWE validation effort in the Western CONUS, observational snow cover data were derived from the NRCS SNOTEL network. SNOTEL stations are generally located in remote high-mountain watersheds in areas that favor high snow accumulation and long snow cover durations. SNOTEL stations report SWE in tenths of inches, measured via a pressure-sensing snow pillow, along with other metrics that vary by station. Daily estimates of SWE are reviewed by NRCS personnel for quality (*nrcs.usda.gov/wps/ portal/wcc/home/aboutUs/monitoringPrograms/ automatedSnowMonitoring*). Also used in this study is a 10m resolution digital elevation model (DEM), employed for the evaluation of both the UA SWE dataset and the numerical results of spatially distributed calculations used to create the Snow Regime Classification system. Both evaluations sub-set the data by elevation bands determined from the US Geological Survey (USGS) 3D Elevation Program (3DEP) 10-Meter Resolution DEM. This is a seamless 3DEP DEM dataset with full coverage for CONUS at a ground spacing of 10 meters north/south and variable east/west spacing due to convergence of meridians with latitude (*developers.google.com/earth-engine/datasets/catalog/ USGS_3DEP_10m*).

After the spatially distributed calculations were sub-set by elevation, they were also divided by spatial domain before being evaluated, using the USGS's Watershed Boundary Dataset (WBD) for more relevant comparisons. The WBD is a comprehensive aggregated collection of hydrologic units (HU) consistent with the national criteria for delineation and resolution. It defines the areal extent of surface water drainage to a point except in coastal or lake front areas where there could be multiple outlets. Watershed boundaries are determined solely upon science-based hydrologic principles, not favoring any administrative boundaries or agency. The HUs are delineated at 1:24,000-scale for CONUS and given a Hydrologic Unit Code (HUC) that describes where the unit is located and the level of the unit. Lower level HUCs cover larger areas than higher level ones, i.e., the higher the level, the more digits to the HUC, since they nest within the previous levels. For this study, we use the lowest level and therefore most coarse scale HUC to parse the results of this study for evaluation of the anomalies, which is HUC02 (*developers.google.com/ earth-engine/datasets/catalog/USGS _WBD_2017_HUC02*).

3 Methods

In order to create the Snow Regime Classification system for CONUS and detect changes in snowmelt cycles over the last 40 years (1981 to 2020), the datasets in our study were quantified and evaluated as average decadal and 30-year normal maps with a 4km spatial resolution. The Snow Regime Classification maps were also generated as downloadable annual GeoTIFF maps, spanning the spatial extent of CONUS. All years in this study are expressed as the water year, which runs from 1 October of the previous year through 30 September of the year label. For

example, water year 1995 consists of data from 1 October 1994 through 30 September 1995 and analogously, the 1990s decade includes 1 October 1989 through 30 September 1999. Since the UA SWE dataset begins on water year 1982 (first SWE date is 1 Oct 1981), the 1980s decade is slightly shorter than the others, consisting of 8 years instead of 10 (starting in 1981 instead of 1979). The 30-year normal dataset analyzed in this study spans water years 1991 through 2020.

The 4km scale PRISM precipitation reanalysis data, 10m resolution USGS 3DEP DEM, and USGS WBD HUs were accessed and examined using Google Earth Engine (GEE). GEE integrates a cloud-based computing environment for geospatial analysis with co-located satellite imagery and climate reanalysis data (Gorelick et al., 2017). All the datasets accessed via GEE in this study are pre-calibrated and fully archived with pixel-scale co-registration of all scenes (Gorelick et al., 2017).

The UA SWE dataset was acquired from the National Snow and Ice Data Center (NSIDC) as daily 4km gridded NetCDF (Network Common Data Form) files for annual water years 1982 through 2020. Since GEE does not recognize or process NetCDF files, these were converted to GeoTIFF spatial files using the R statistical programming application, version 4.2.1 (*www.r-project.org/*) and R package daymetr V1.6 (Hufkens, *cran.rproject.org/web/packages/daymetr/*). Subsequently, the converted UA SWE files were uploaded into GEE as annual images with 365 bands per image representing the daily values of SWE expressed in mm depth of water for each 4km grid cell across CONUS. For a flow chart of study methods, refer to ***Figure S1*** in ***Supporting Information for Changing Snow Regime Classifications across the Contiguous United States.***

3.1 Gridded SWE Dataset Evaluation

To perform a dataset-agnostic evaluation of the data used in this study, an array of simple snow cover metrics were derived from the UA SWE data and summarized both spatially and graphically. These snow cover metrics were summarized through the use of average decadal and 30-year normal maps of CONUS, as well as with graphical analysis of the values assembled and quantified by elevation. The snow cover metrics generated for the gridded dataset summary include maximum SWE (mm), SCD (number of days), and dates of first accumulation, end of ablation, and maximum SWE (all expressed as day of water year or DOWY).

First, for each water year from 1982 through 2020, these six snow cover metrics were derived annually from the UA SWE images that were originally imported into GEE with 365 daily values (bands) and an associated DOWY for each SWE value. For leap years during the period of study, the UA SWE images had 366 daily bands, including an additional SWE value for February 29th, which was incorporated into calculations of the snow metrics for those years accordingly. New annual images were generated for each water year, each with six bands corresponding to the six summary values or metrics in each 4 km pixel; (1) max SWE, (2) SCD, (3) first accumulation, (4) last ablation, (5) max SWE date, and (6) a categorical flag if there was zero SWE (no snow) on April 1st. While calculating accumulation and ablation DOWY values, the last 45 days of the water year (15 August through 30 September) were excluded from consideration. This was to ensure that new events of early accumulation in late August or September were not mistakenly detected as false start of ablation dates. A late August start of accumulation date can occasionally occur at the highest elevations of some CONUS mountain ranges (Trujillo & Molotch, 2014).

For very warm areas in southern CONUS, where grid cells never had a SWE value above zero for the entire year, these pixels were masked, making all values null for the six snow cover

metrics. Furthermore, areas with trace amounts of annual SWE, deemed negligible for our analysis, were also masked. Pixels were considered to have negligible snow cover and masked (assigned null values for the six metrics) if they contained three weeks (21 days) or fewer with SWE values greater than zero for a given water year for the annual maps (images). Within the regions containing significant annual SWE (more than 21 days), grid cells with a zero value for SWE on April 1st were extracted separately as an additional discrete categorical band. These pixels are of special interest, as they appear to contradict the nearly century-old convention (Burton, 1916; Cayan, 1996; Fisher, 1918) in the western US that April 1st SWE represents total seasonal accumulation and can be used as a surrogate for maximum seasonal snowpack (Bohr & Aguado, 2001; Musselman et al., 2019; Wrzesien et al., 2017).

The next step involved calculating the decadal and 30-year normal averages of the six snow cover metrics in order to generate summary maps for CONUS. Pixels with 21 days of snow cover or less in all ten years of a decade (all 30 years in the normal) were masked, given null values, and given the categorical label "negligible" in the decadal maps. Pixels with 21 days of snow cover or less annually, in five years or more (half the decade or more) were also masked and given null values in the decadal maps, but given a categorical label of "intermittent". The "intermittent" threshold for the 30-year normal map is 15 years or more (half the normal period).

Finally, we considered the remaining pixels that had at least six years and up to nine years with substantial snow cover (more than 21 days annually) important enough to have their snow metric values represented in the decadal maps. This was done by averaging values on years with substantial snow cover (more than 21 days) and leaving out the years that would have been labeled "negligible" on the annual maps (21 days of snow or less). We did not use zero values in the negligible pixels, opting instead to exclude them in the decadal average calculations by assigning null values, because this study focuses on changes over the study period in regions with seasonal snow cover. Regions with negligible or ephemeral snow cover don't source enough of their annual water budget from snowpack to be of concern for this study.

A similar approach was taken regarding the areas with zero SWE on April 1st for the decadal average and 30-year normal summary maps. The zero April 1st SWE band for the decadal images includes only those pixels with no SWE on April 1st for at least half the decade (5 years) or longer, within the areas deemed to have significant SWE (more than three weeks of SWE for more than half the decade). A 15-year threshold was employed for the 30-year normal zero April 1st snow cover metric.

Additionally, a modest collection of 82 in-situ snow cover observations, from six weather stations across CONUS were selected for use as an empirical spot check to ground-truth the zero April 1st UA SWE values. Each station is part of either the WBAN or SNOTEL station network (see section ***2 Data Sources***) and co-located within 4km grid cells of the UA dataset that had zero April 1st SWE for select years in each decade. Spot checks were performed in six grid cells across representative regions of CONUS with the corresponding weather station, including New England (WBAN Station USW00014764), the Northeast (WBAN Station USW00014733), Midwest (WBAN Station USW00014922), Rocky Mountains (SNOTEL Site 708), Sierra Nevada Mountains (SNOTEL Site 778), and the Pacific Northwest (SNOTEL Site 420). We validated whether or not on-the-ground stations reported no snow cover on April 1st in the same years as the UA SWE data.

The final component of our dataset-agnostic evaluation involved sub-setting maximum SWE (mm) and SCD (days) by elevation. The USGS 3DEP 10m DEM was partitioned into 200m and 400m wide elevation bands for the entire span of elevations across CONUS. Then the decadal average snow metrics located within each elevation band were averaged. Specifically, maximum SWE and SCD were averaged on the 200m elevation scale, with 21 bins from 0m to 4200m for each decade, while dates of accumulation, ablation, and maximum SWE were averaged on the 400m elevation scale, with 10 bins per decade.

3.2 Snow Regime Classification System

To create the Snow Regime Classification system, SWE to precipitation ratios were calculated across CONUS, using the UA SWE and PRISM precipitation datasets and thresholding the numerical results into discrete classes. These discrete Snow Regime Classifications include rain dominated (RD), snow dominated (SD), transitional (R/S), and perennial snow (PS).

The UA SWE files that were converted from NetCDF to GeoTIFF and uploaded into GEE as annual images, representing the daily values of SWE (in mm) for each water year from 1982 to 2020, were utilized to derive the value for the numerator of the snow classification thresholding ratio. Tohver et al. (2014) used April 1st SWE values in this ratio to characterize hydrologic regimes of the PNW. Therefore, in this study, the April 1st SWE value from each water year of the analysis period (1982-2020) for each 4 km pixel across CONUS was extracted on a pixel by pixel basis for input into the classification ratio. Alternatively, a second approach was also engaged wherein a uniquely determined maximum annual value of SWE for each pixel across CONUS was also extracted on a pixel by pixel basis.

For the denominator of this ratio, cumulative cool season (October through March) precipitation (also in mm) was calculated from the PRISM data for each water year of the analysis period in each 4 km pixel across CONUS. Next, the pixel-wise spatial calculation of SWE divided by cumulative precipitation was performed within each 4 km pixel across the entire spatial extent of CONUS as:

$$Class\ Threshold\ Ratio\ = \frac{SWE(mm)}{Cumulative\ cool\ season\ precipitation\ (mm)} \qquad \text{Eqn. (1)}$$

This calculation was done for both April 1st and maximum SWE values. For each resultant spatial dataset of the ratios throughout CONUS, for each water year, a thresholding approach was applied in order to translate the numerical data into discrete categories for each snow regime class for the two ratio methods. Building upon classifications defined by Tohver et al. (2014) for RD, R/S, and SD, we also developed an additional classification for perennial snow (PS) areas. The thresholds used in this study are:

Ratio < 0.1: Rain Dominated (RD)

Ratio = 0.1 to 0.4: Transitional (R/S)

Ratio = 0.4 to 1.0: Snow Dominant (SD)

Ratio > 1.0: Perennial Snow (PS)

To further constrain the PS regime and increase its accuracy, areas with ratio values over 1.0 were also verified by confirming that each pixel had at least 0.5mm of SWE on the first day of the water year (October 1st), as this is necessary for an area to be classified as having year-round snow cover. Areas with ratios over 1.0, but no SWE on October 1st were assigned ratio values of

0.9 and subsequently classified as SD instead. These areas were typically located in drier regions of CONUS with low precipitation represented by the PRISM data. The Snow Regime Classifications for CONUS, using the maximum SWE value ratio approach, are available for each year of the analysis as downloadable GeoTIFF files (see the link at the end of this document in *Research Product Availability*).

The same approach taken for the annual classification maps was also employed to generate decadal average (and 30-year normal) classification maps. These representative maps are used to summarize the results of our study. Snow Regime Classification anomalies by decade were derived for both the April 1st SWE and maximum SWE ratio approaches. These anomalies were calculated as the departures from their respective 30-year normals for each decade and recognized as a shift in snow regime classification. For any 4km pixel in each decade, if the classification did not match that of the respective 30-year normal, it was considered an anomaly and also characterized as a shift to either a warmer class with a greater proportion of liquid precipitation or a colder class with more solid precipitation. Essentially, this means that changes from RD to R/S or SD, and from R/S to SD mean more solid precipitation. Changes from SD to R/S or RD, and from R/S to RD mean a shift to more liquid precipitation.

3.3 SWE Input Data Comparison

We also performed a comparison of spatial extents for Snow Regime Classifications across CONUS using both the April 1st SWE and maximum SWE. Areas of the pertinent classifications in each decadal map, including RD, R/S, and SD, were calculated in m^2 for both SWE to cool season precipitation ratios, along with their respective 30-year normals. PS areas were found to be relatively small for CONUS in the average decadal maps, and therefore, not reported here. Percent departures in area from the 30-year normal were calculated for each class in each decade, for both ratio approaches. The percent departures were calculated as:

$$\%\ Area\ Departures = \frac{Class\ Area_{Decadal\ Avg} - Class\ Area_{30\text{-}yr\ Norm}}{Class\ Area_{30\text{-}yr\ Norm}} * 100\% \qquad \text{Eqn. (2)}$$

To aid in the interpretation of the percent departures in area from the 30-year normal for the snow regime classifications, a temperature analysis was performed using gridded temperature from the PRISM dataset. Daily mean air temperatures in each 4 km grid cell were taken directly from PRISM and averaged over both annual and cool season (October through March) temporal extents. Then overall average annual air temperatures across CONUS were calculated for each water year in our study period (1982-2020), as well as for each decade, and the 30-year normal (1991-2020). The same was also done for the cool season months only. For each water year, temperature anomalies were then calculated as the departures from the 30-year normal as well as from the respective decadal average. These anomalies were calculated for both annual and cool season average air temperatures for each water year. Certain years were highlighted if air temperatures could have contributed to differences in spatial extents of certain snow regime classifications from decade to decade. This was done by targeting anomalies that were more than 0.9 degrees Celsius colder or warmer for either the annual or cool season statistics.

Finally, a comparison of the raw numerical results from the calculations of the two ratio approaches was done. Two numerical values, one each for the April 1st and maximum SWE to cumulative cool season precipitation ratios, were calculated in each 4km pixel for each decadal average SWE and precipitation value, as well as for the 30-year normal. In other words, the

spatially distributed calculations resulted in each pixel across CONUS containing 10 values. Maps of these ratio calculations for each decade and the 30-year normal (before they were thresholded into the discrete categorical snow regimes) were segmented by HUC02 WBD across CONUS. Within each HUC02 area, further sub-setting of the region was done by 200m elevation bands using the USGS 3DEP 10m DEM. For each elevation band within each HUC02, the ratio values were averaged for both the April 1st and maximum SWE methods of calculation. This was done for each decade and the 30-year normal. The results of assembling and averaging the raw numerical values in this manner were then compared graphically for the two ratio techniques employed in this study.

4 Results

4.1 Gridded SWE Dataset Evaluation

The UA SWE included decadal average maps used as spatial summaries for several snow cover metrics derived from the SWE information. An overview, summarized across the large spatial extent of CONUS, for the 1980s through the 2010s and for the 30-year normal, includes maps of maximum SWE values in mm (***Figure 1a***), SCD in number of days (***Figure 1b***), first date of snow accumulation (DOWY) (***Figure 2a***), and last date of snow ablation (DOWY) (***Figure 2b***). These maps also show regions of CONUS deemed as having intermittent snow cover, which included areas with less than 3 weeks of SWE annually for at least half the decade (5 years) or at least 15 years for the 30-year normal (***Figure 1b***).

Another snow metric used to describe and evaluate the UA SWE dataset was the spatial extent of areas with zero SWE values on April 1st for at least half the decade (5 years). For the decadal average maps, the zero April 1st SWE areas were found within regions of CONUS with significant snow cover (***Figure 3***). An on-the-ground spot check was also performed for the zero April 1st SWE maps, to see if a small collection of in-situ weather stations were also reporting no snow cover on the same dates in the same locations (***Figure 3***). A small sample of 82 UA pixels reporting zero April 1st SWE were used in this spot check. The pixels are distributed temporally over the four decades in our study period and spatially across CONUS at six pixels co-located with six weather stations (***Figure 3***). We found an 83% agreement between the modeled and observational data points with 62 weather station observations confirming that there was no snow cover out of the 82 UA SWE pixels indicating the same (***Figure 3***). Since the CONUS-wide maps span such a large spatial domain, a brief visual evaluation shows magnitudes of values staying somewhat geographically stable throughout the decades. However, upon closer inspection, these snow metrics vary significantly at the regional scale, from decade to decade (***Figures 1, 2,*** and ***3***).

Animated movies of annual maps of these snow cover metrics across CONUS for the 39 water-year study period (1982 to 2020) can be viewed in ***Supporting Information for Changing Snow Regime Classifications across the Contiguous United States.*** In the supporting information, annual maps of maximum SWE values, maximum SWE dates, SCD, first date of snow accumulation, last date of snow ablation, and areas with zero April 1st SWE, are listed as ***Data Sets S1, S2, S3, S4, S5, and S6,*** respectively.

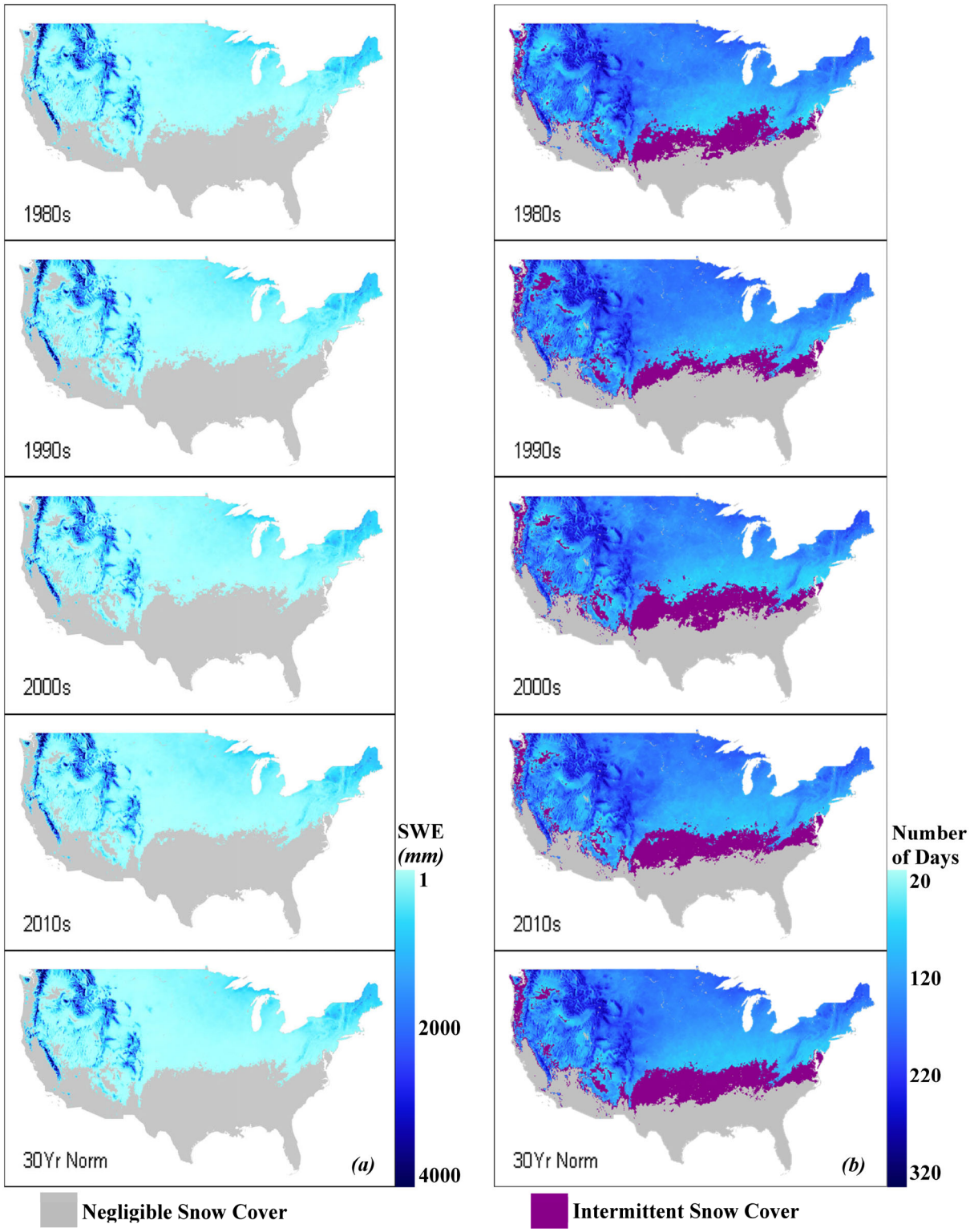

Figure 1. Average maximum SWE (***a***) and average snow cover duration (***b***) by decade and by 30-year normal from the per pixel analysis of the UA SWE. Negligible snow cover includes pixels with less than 3 weeks of SWE annually for half the decade (5 years) or longer (15 yrs for 30-yr norm). Intermittent snow cover shows pixels within the negligible region that had at least one year with more than 3 weeks of SWE.

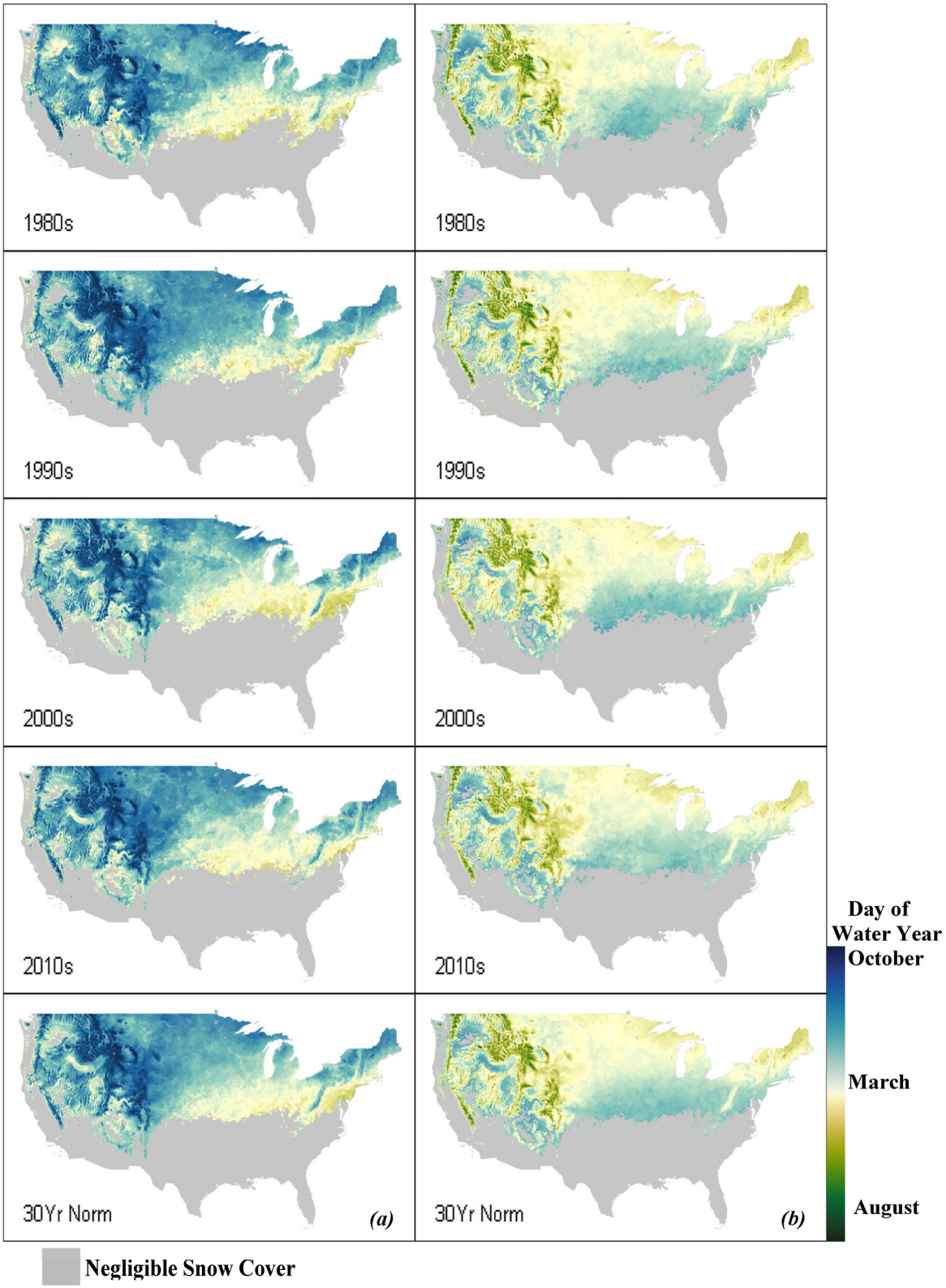

Figure 2. First date of snow accumulation (***a***) and last date of snow cover ablation (***b***) by decade and by 30-year normal from the per pixel analysis of the UA SWE. Negligible snow cover includes pixels with less than 3 weeks of SWE annually for half the decade (5 years) or longer (15 years for 30-yr normal).

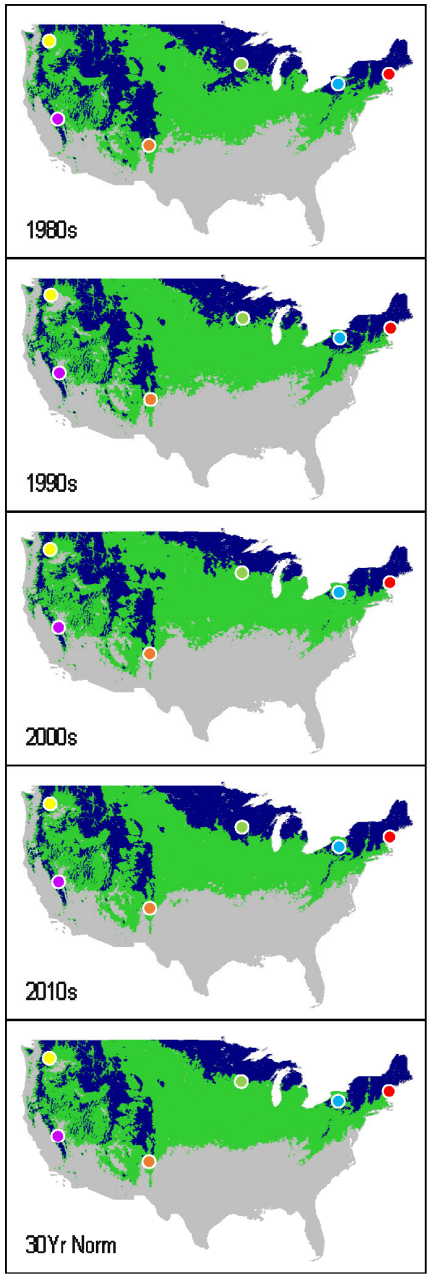

Region	Weather Station	State / Elevation	Zero Apr 1st UA SWE Yrs Station Agreement (*Y/N*)
New England	Portland International Airport USW00014764	Maine 14 m	1985 *N* 1986 *Y* 1988 *Y* 1991 *Y* 1995 *Y* 1998 *Y* 1999 *Y* 2002 *Y* 2003 *Y* 2004 *Y* 2006 *Y* 2010 *Y* 2013 *Y* 2016 *Y* 2020 *Y*
		Totals: ***Y=14 N=1***	% Agreement = ***93%***
Northeast	Buffalo Niagara International Airport USW00014733	New York 211 m	1982 *Y* 1985 *Y* 1986 *Y* 1988 *Y* 1990 *Y* 1995 *Y* 1997 *Y* 1998 *Y* 2003 *Y* 2005 *Y* 2007 *Y* 2009 *Y* 2012 *Y* 2013 *Y* 2017 *Y* 2018 *Y*
		Totals: ***Y=16 N=0***	% Agreement = ***100%***
Midwest	Minneapolis St. Paul Int'l Airport USW00014922	Minnesota 255 m	1985 *N* 1986 *Y* 1987 *Y* 1988 *Y* 1991 *Y* 1994 *Y* 1998 *Y* 1999 *Y* 2003 *Y* 2004 *Y* 2006 *Y* 2007 *Y* 2012 *Y* 2015 *Y* 2016 *Y* 2017 *Y*
		Totals: ***Y=15 N=1***	% Agreement = ***94%***
Rocky Mountains	Quemazon SNOTEL Site # 708	New Mexico 2898 m	1986 *N* 1989 *N* 1999 *Y* 2002 *Y* 2004 *Y* 2006 *Y* 2007 *N* 2011 *Y* 2014 *Y* 2016 *Y* 2017 *Y*
		Totals: ***Y=8 N=3***	% Agreement = ***73%***
Sierra Nevada Mountains	Spratt Creek SNOTEL Site # 778	California 1848 m	1988 *Y* 1990 *Y* 1992 *Y* 1994 *Y* 2001 *Y* 2003 *Y* 2004 *Y* 2007 *Y* 2012 *Y* 2013 *Y* 2015 *Y*
		Totals: ***Y=11 N=0***	% Agreement = ***100%***
Pacific Northwest	Cougar Mountain SNOTEL Site # 420	Washington 975 m	1983 *Y* 1984 *N* 1986 *N* 1987 *N* 1992 *Y* 1994 *N* 1998 *N* 2003 *N* 2005 *Y* 2007 *N* 2015 *Y* 2016 *N* 2019 *N*
		Totals: ***Y=4 N=9***	% Agreement = ***31%***

Zero April 1st SWE agreements - Stations vs UA SWE: 68 / 82 points = 83 %

Figure 3. Areas with zero SWE on April 1st by decade and by 30-year normal (1991-2020), resultant from per pixel analysis of the UA data. Negligible snow cover includes pixels with less than 3 weeks of SWE annually for half the decade (5 years) or longer, while Significant includes those for 4 years or less. Zero April 1st SWE areas include pixels with SWE equal to zero on April 1st for half the decade (5 years) or longer, within the significant snow cover areas. A 15 year threshold for the 30-year normal was used for both negligible and zero April 1st snow cover. The chart indicates empirical spot checks for select weather stations in zero April 1st UA SWE areas. A "Y" indicates there is agreement between the UA SWE pixel and the observational location, while an "N" indicates there is not agreement.

The final evaluation of the UA SWE involved quantitative graphical analysis of average decadal and 30-year normal snow metrics by elevation, including maximum SWE (mm) and SCD (days), and dates of first accumulation, end of ablation, and maximum SWE (all in DOWY) (***Figure 4***). In ***Figure 4a***, maximum SWE and SCD are shown in the graph to vary by 200m elevation band, while in ***Figure 4b***, the decadal average and 30-year normal start of accumulation and end of ablation dates are displayed as bar graphs for each decade, within each 400m elevation band. Also seen in ***Figure 4b*** is the 30-year normal maximum SWE for each 400m band.

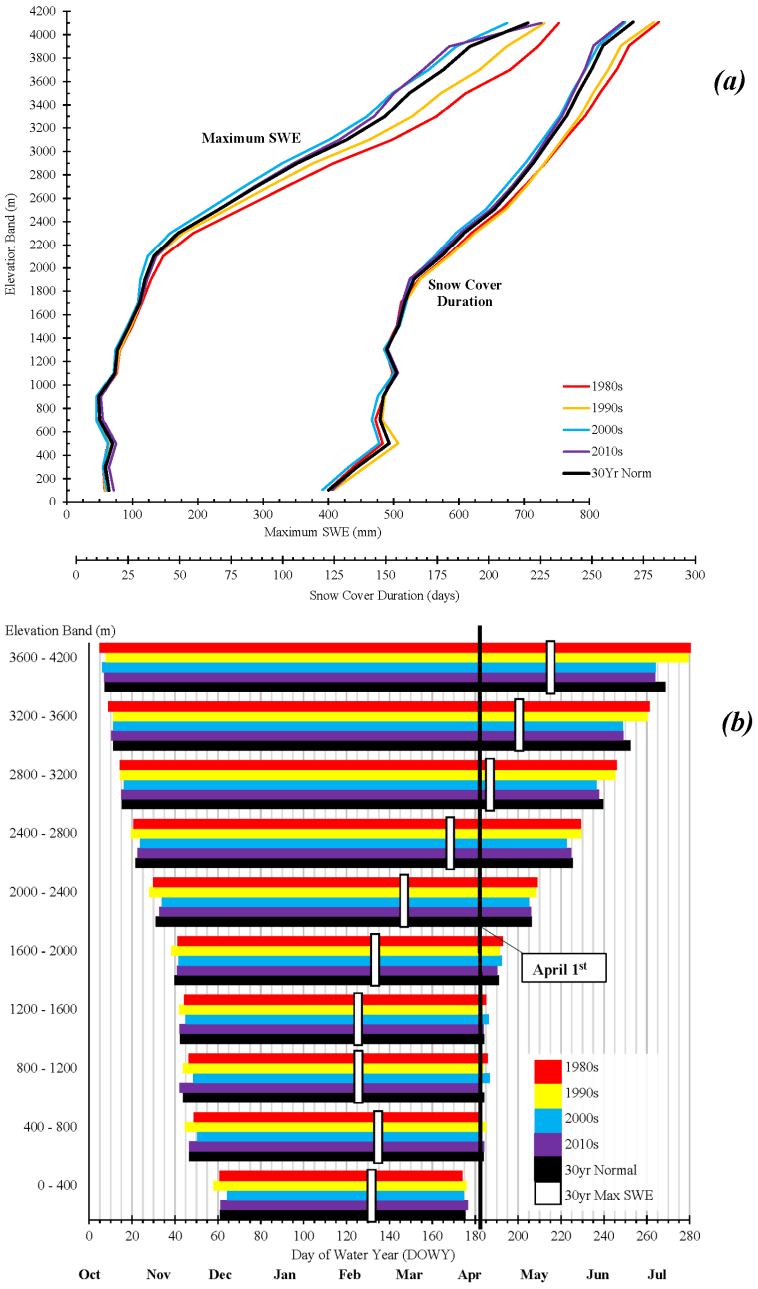

Figure 4. Decadal and 30-year normal (1991-2020) per pixel analysis of the UA SWE dataset by elevation bands. ***(a)*** Average max SWE values (mm) and SCD (days) by 200m band. ***(b)*** Average start of accumulation, end of ablation, and max SWE dates (days) by 400m band. ***Note:*** lines in ***(a)*** do not reach zero on elevation axis (y-axis) because each SWE value is an average per band, therefore SWE values are placed in middle, *i.e.* at 100m for 0m to 200m. Also note values are averaged across pixels meeting the minimum decadal SCD (≥ 3 weeks SWE annually, ≥ 5 years / decade).

4.2 Snow Regime Classification System

The results of the Snow Regime Classification, using the dual approach of April 1st and maximum SWE over precipitation ratios for thresholding, yielded quite different results for the two methods. These differences are evident in the divergent spatial extents of the snow regime classes in both the decadal averages (***Figure 5***) and the 30-year normal (***Figure 6***). The snow regime class anomalies (***Figure 7***), i.e., the departures from their respective 30-year normal classes (***Figure 6***), are categorized by the shift in precipitation phase (proportionally more liquid or solid precipitation than the 30-year normal). RD to R/S or SD, and R/S to SD mean a shift to more solid precipitation. SD to R/S or RD, and R/S to RD mean a shift to more liquid precipitation.

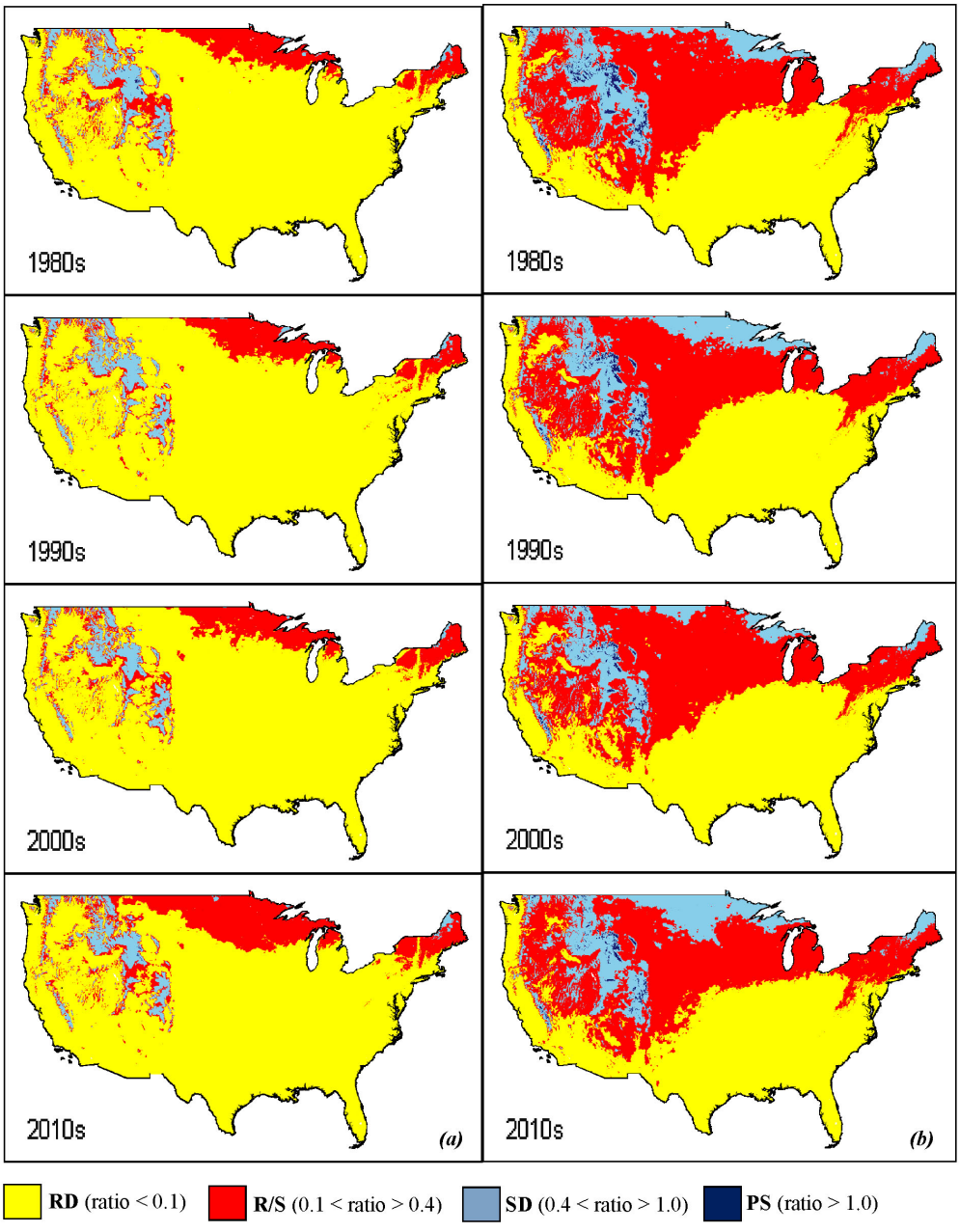

Figure 5. Snow Regime Classification by decade using ***(a)*** April 1st SWE / cumulative cool season precipitation (Oct through Mar) and ***(b)*** Maximum SWE / cumulative cool season precipitation (Oct through Mar) as thresholding ratios for the regime classes of rain dominated (RD), transitional (R/S), snow dominated (SD), and perennial snow (PS).

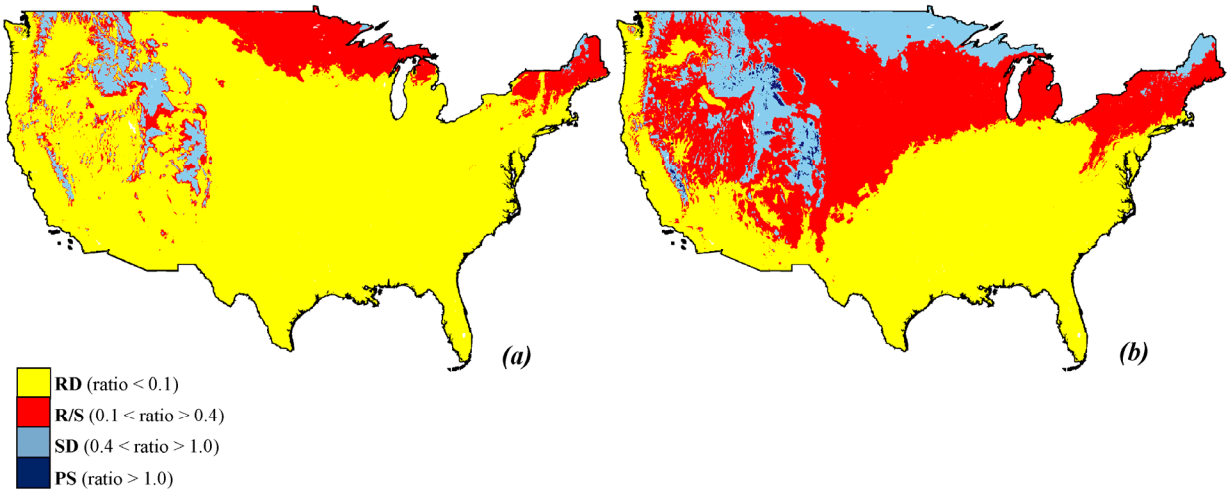

Figure 6. Thirty-year normal (1991-2020) Snow Regime Classifications derived from ***(a)*** April 1st SWE / cumulative cool season precipitation (Oct through Mar), and ***(b)*** Maximum SWE / cumulative cool season precipitation (Oct through Mar). Ratios were used for thresholding the regime classes of rain dominated (RD), transitional (R/S), snow dominated (SD), and perennial snow (PS).

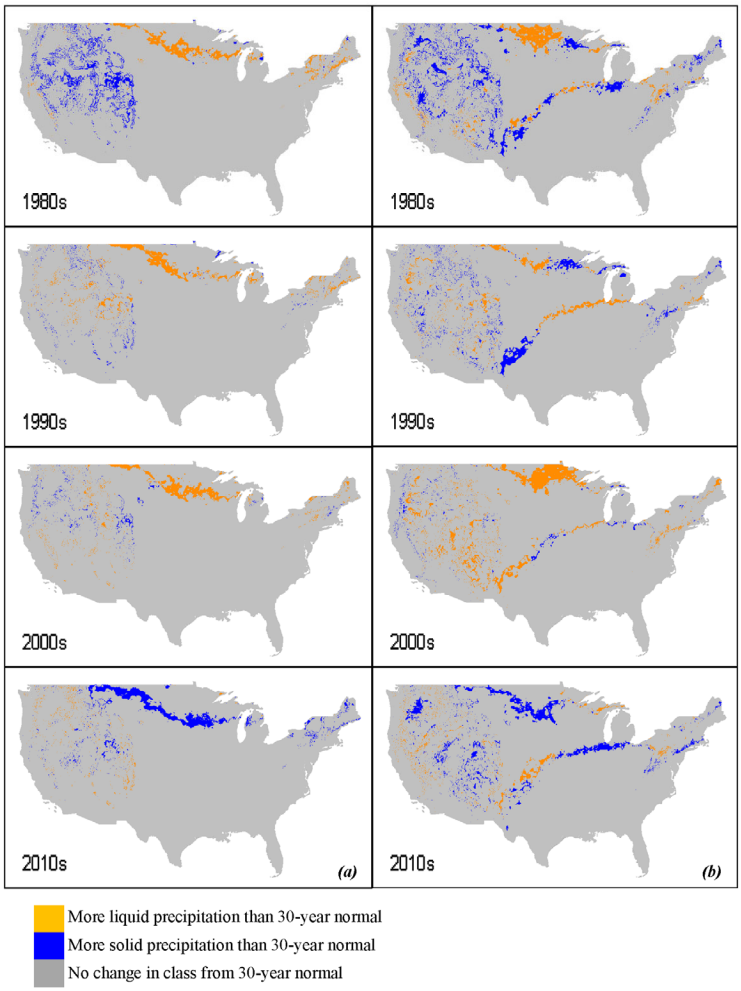

Figure 7. Snow Regime Classification Anomalies in (***a***) April 1st SWE ratio and (***b***) Maximum SWE ratio approaches. Departures from 30-year normals by shift in class; RD to R/S or SD, and R/S to SD indicate a shift to more solid precipitation. SD to R/S or RD, and R/S to RD indicate a shift to more liquid precipitation.

Animations of annual Snow Regime Classifications for the study period (1982 to 2020) can be viewed in ***Supporting Information for Changing Snow Regime Classifications across the Contiguous United States***, using the thresholding ratios of April 1st and maximum SWE over cumulative cool season precipitation (Oct through Mar), as ***Data Sets S7 and S8***, respectively.

4.3 SWE Input Data Comparison

Results of the quantitative evaluation for each of the two thresholding ratio techniques for generating the Snow Regime Classifications include a comparison of calculated areal extents for the RD, R/S, and SD classes in each decade (***Figure 8***), a temperature analysis using the PRISM dataset (***Figure 9***), and a comparison of the numerical results from the ratio calculations per elevation band in relevant HUC2 regions (***Figure 10***). In ***Figure 8***, the decadal anomalies, or percent departures from 30-year normals, in snow regime class extents, indicate a continued decrease in SD areas for both the April 1st and maximum SWE ratio methods, during the 1980s, 1990s, and 2000s, with a rebound in the 2010s. In ***Figure 9***, the last decade in our study period (2010s), also shows the most variation in PRISM derived average air temperatures from the 30-year normals. For both year-round (12 month) annual average air temperatures across CONUS, as well as for cool season (October through March) annual average air temperatures, there are more anomalies (departures from their respective normals) than in any other decade.

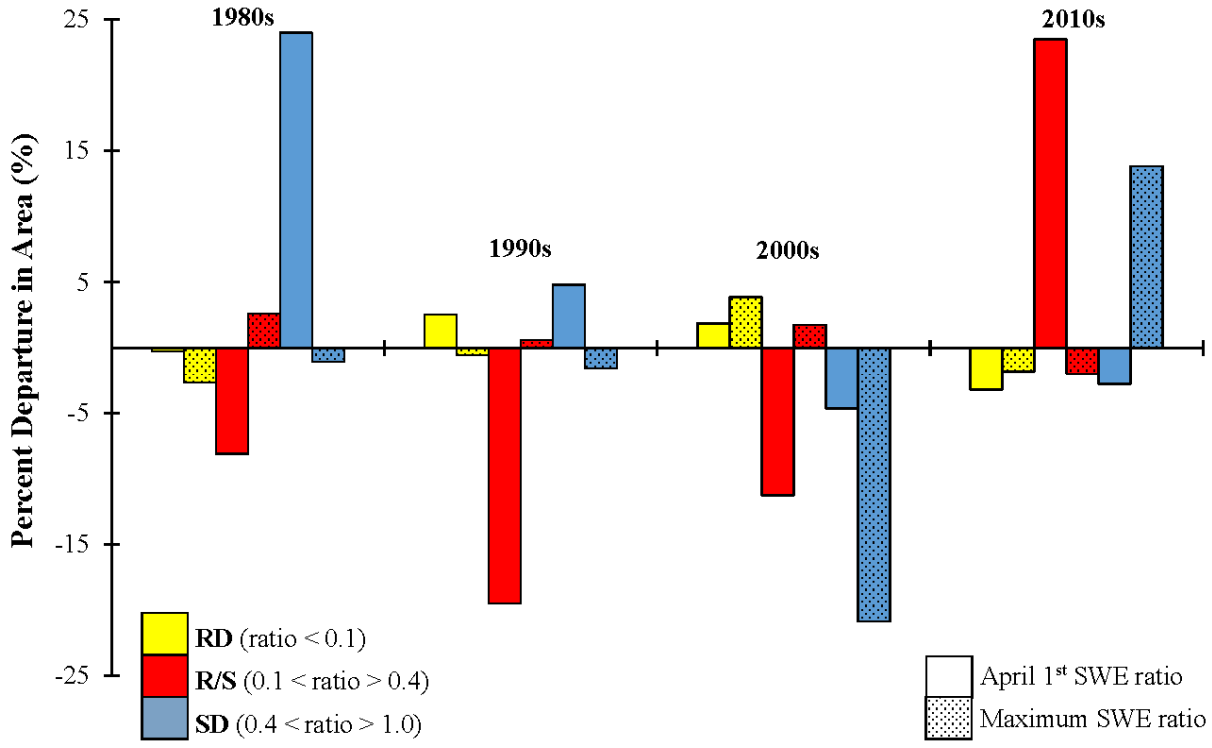

Figure 8. Percent departures in areal extents from the 30-year normals (1991-2020) for the pertinent Snow Regime Classifications (RD – rain dominated, R/S – transitional, and SD – snow dominated) as a comparison between the two ratio thresholding techniques; April 1st SWE ratio vs. Maximum SWE ratio.

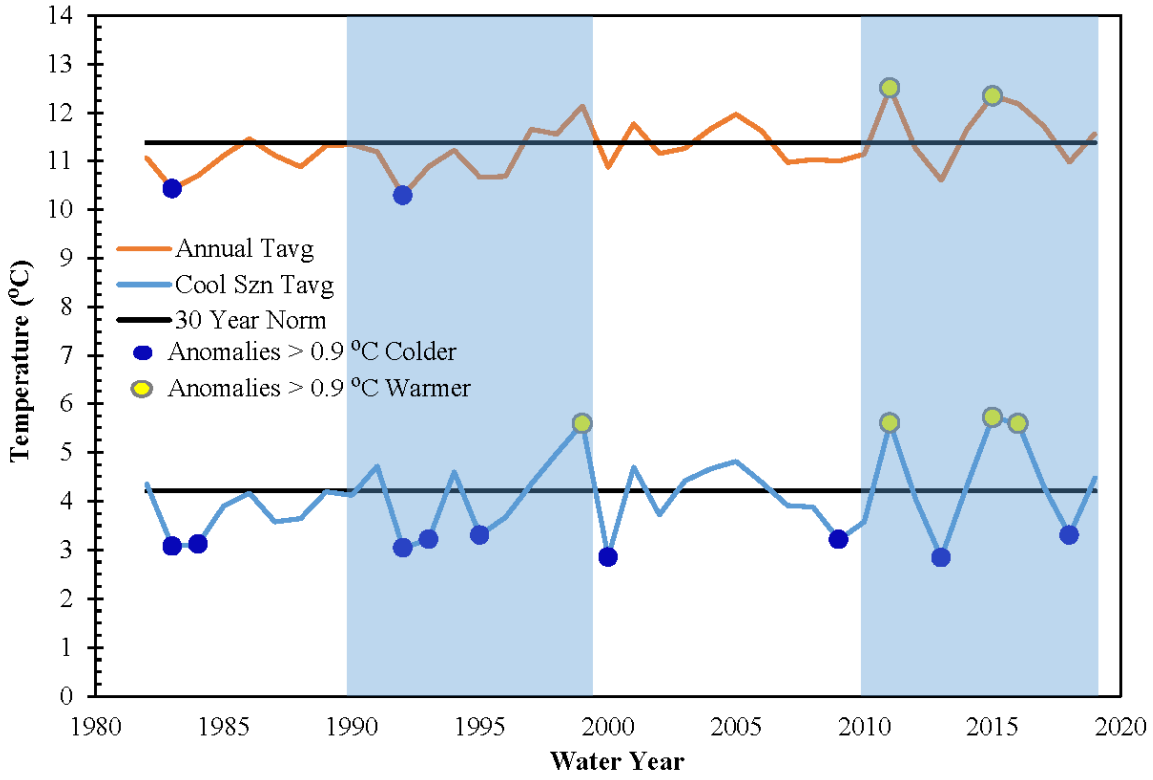

Figure 9. PRISM temperature analysis for water years 1981 to 2020 across CONUS, with annual averages compared to cool season (Oct through Mar) averages and respective 30-year (1991 – 2020) average temperatures. Air temperature anomalies (departures from 30 year normal) show values deviating by 0.9 degrees Celsius or more.

The map at the top of ***Figure 10***, in the upper left corner, shows the locations of each of the 18 USGS HUC2 regions that make up CONUS. Below this map are the results of regional, elevation dependent analyses of the SWE to precipitation ratio calculations for 15 of the 18 HUC2s. HUC2-03 South Atlantic-Gulf, HUC2-08 Lower Mississippi, and HUC2-12 Texas-Gulf regions, covering Southeast CONUS and the Gulf of Mexico, had negligible SWE and were not included (***Figure 10)***.

These ratios are the quantitative values that were thresholded to derive the Snow Regime Classifications (***Figures 5*** and ***6***). In ***Figure 10***, we sub-set the pixel values spatially by HUC2 and temporally by decade (or 30-year normal). For each HUC2 region and decade (or 30-year normal), the pixels were then sub-set further by 200m elevation band. The two ratio values in each pixel falling into each group (sorted by elevation band, HUC2, and decade) are averaged and plotted in ***Figure 10*** by elevation gradient. Each graph, representing its temporal and spatial location within the data stack, depicts average values of the two ratios and how they vary by elevation. The averaged point values in each 200m elevation range (bin) are connected by lines; with average April 1st SWE ratios in green and average maximum SWE ratios in blue (***Figure 10***).

Raw values of the April 1st SWE ratios are smaller than those of the maximum SWE ratios. However, both sets of values increase with elevation at roughly similar rates; meaning an increase in SWE relative to the respective cool season precipitation in most pixels. Exceptions to this interpretation occur within HUC2-01 New England, HUC2-05 Ohio, and HUC2-07 Upper Mississippi. These particular HUC2 regions, unlike the rest of CONUS, display a backward trend in ratio values at their uppermost elevations, consistently across the decades.

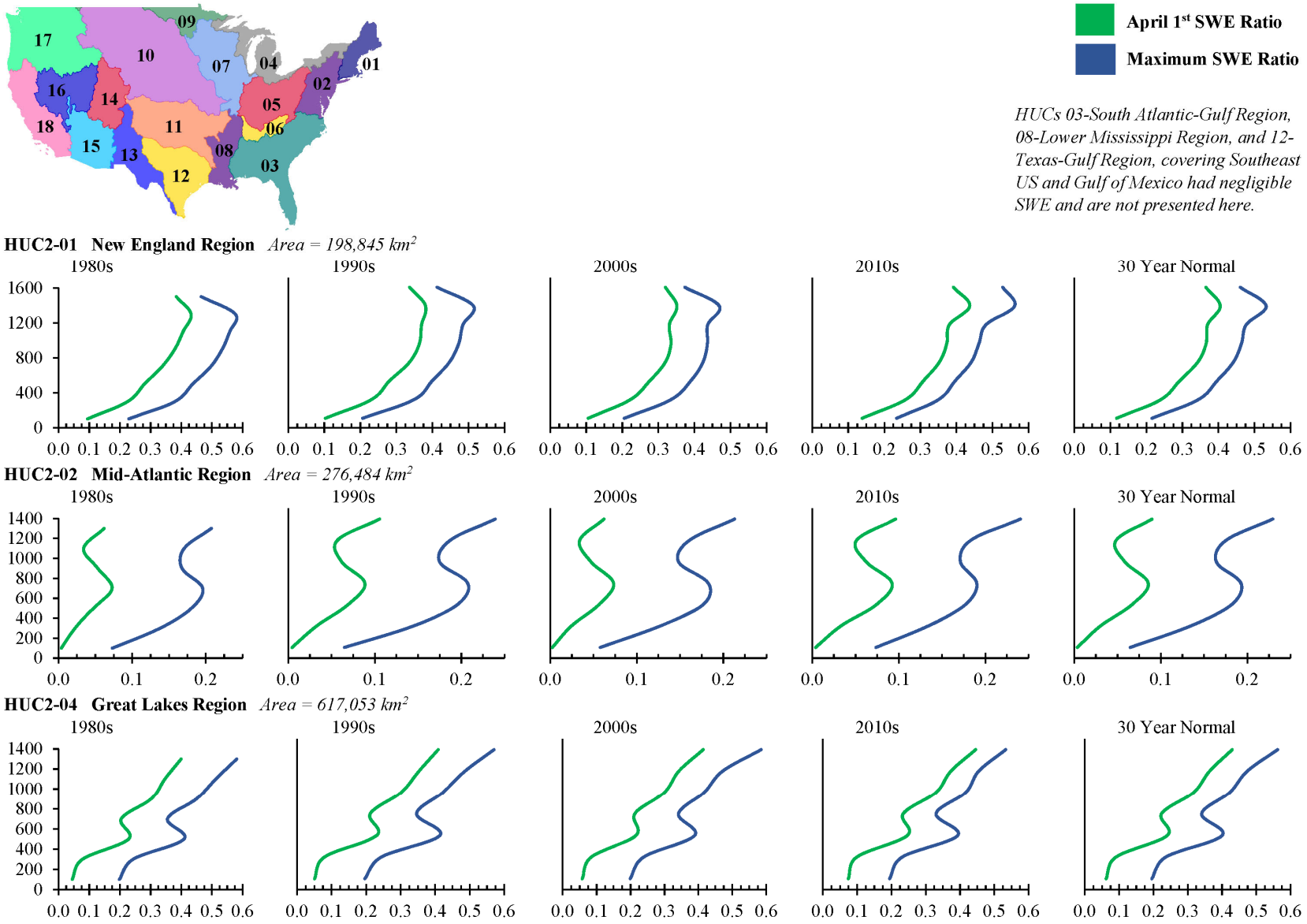

Figure 10a. SWE to cumulative precipitation ratios for two approaches; decadal averages and 30 year normals per 200m elevation bin in relevant HUC2 regions.

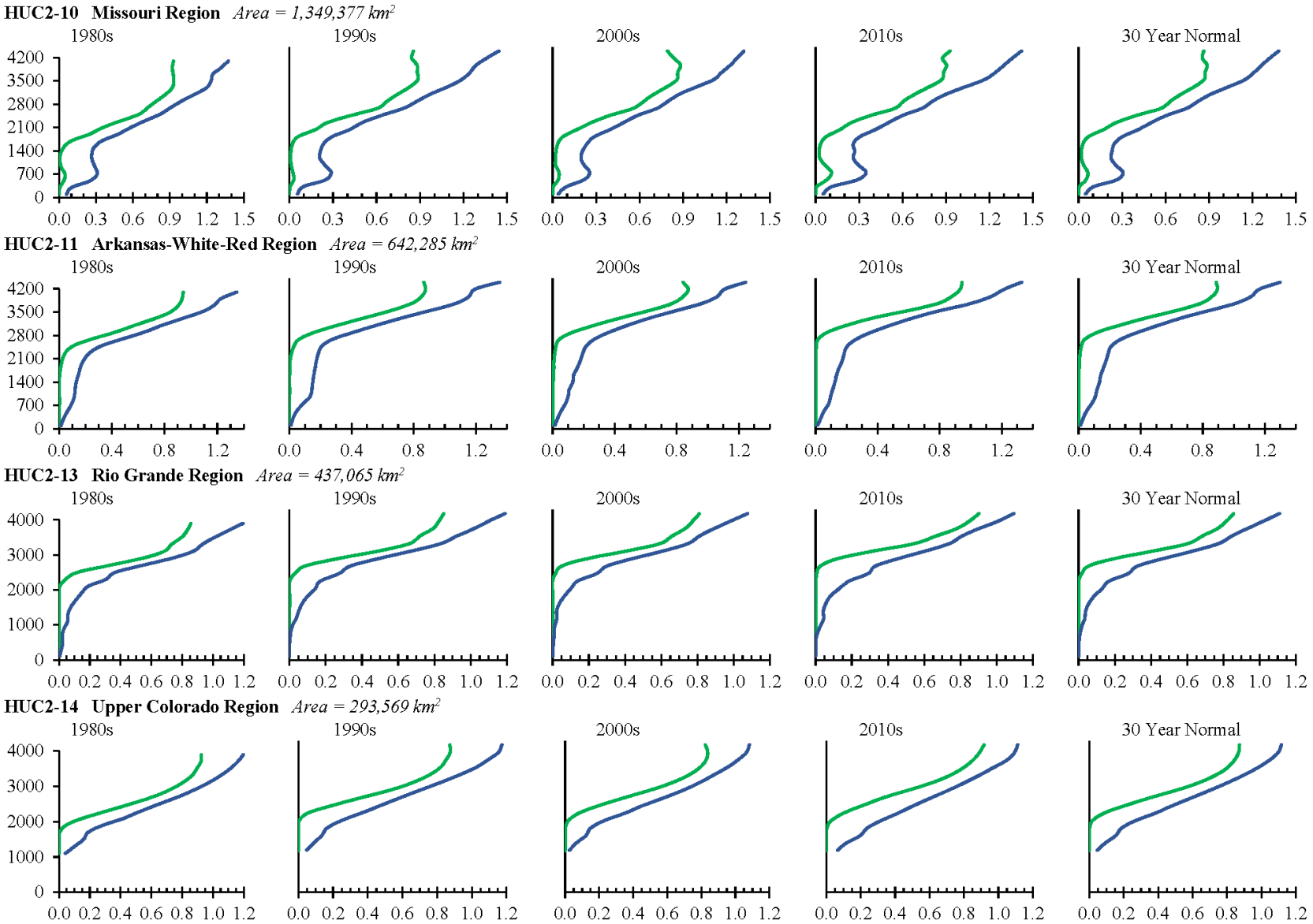

Figure 10b. SWE to cumulative precipitation ratios for two approaches; decadal averages and 30 year normals per 200m elevation bin in relevant HUC2 regions.

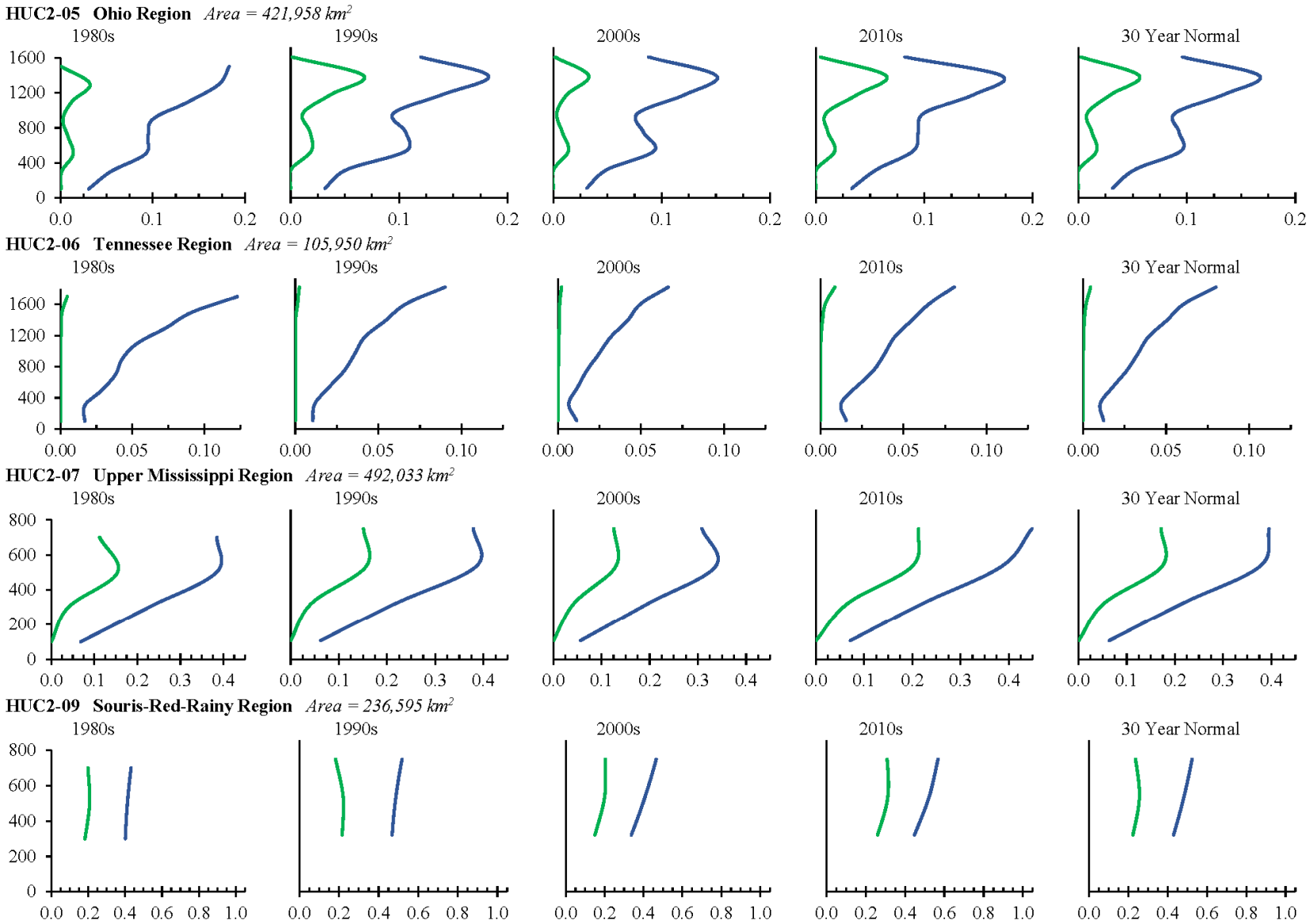

553

554 **Figure 10c.** SWE to cumulative precipitation ratios for two approaches; decadal averages and 30 year normals per 200m elevation bin in relevant HUC2 regions.

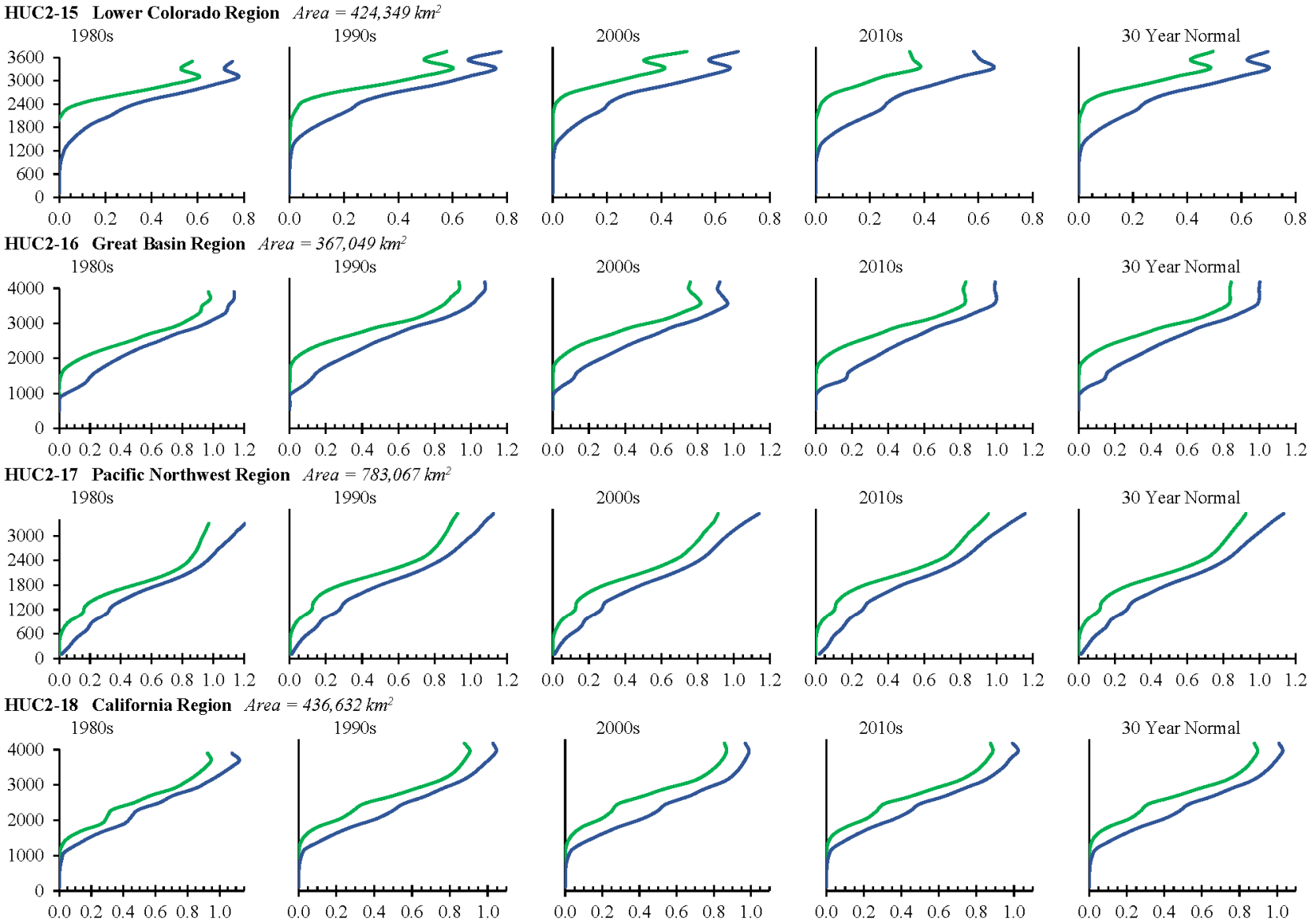

Figure 10d. SWE to cumulative precipitation ratios for two approaches; decadal averages and 30 year normals per 200m elevation bin in relevant HUC2 regions.

5 Discussion

5.1 Gridded SWE Dataset Evaluation

The dataset evaluation includes decadal summary maps of CONUS for average maximum SWE and SCD (***Figure 1***), as well as for first date of accumulation and last date of ablation (***Figure 2***). These maps also show regions with negligible snow cover (less than 3 weeks of SWE annually for at least half the decade) (***Figures 1*** and ***2***) and regions with intermittent snow cover (within negligible regions, at least one year with more than 3 weeks of SWE) (***Figure 1b***). Since these maps span all of CONUS, a brief glance shows values staying fairly stable throughout time, however, there are significant variations over time at the regional scale (***Figures 1*** and ***2***). Over our 40-year study period, analysis of the UA SWE data indicate an overall decline in average decadal maximum SWE values in several large regions of CONUS, from the 1980's through the 2000's, with a slight increase in maximum SWE in the 2010's (***Figure 1a***). Trends in declining snowpack across CONUS, seen in this study's analyses, align with observations from previous studies (Abatzoglou, 2011; Brown, 2000; Knowles, 2015; Mote et al., 2005, 2018) in regions such as the Northeast / New England (Scott et al., 2008), over the Northern Great Plains (Fassnacht et al., 2016), across the Rocky Mountains (Pederson et al., 2013), and in the Pacific Northwest (Mote et al., 2008; Vano et al., 2015) (***Figure 1***).

Another snow metric used to evaluate the UA SWE dataset with decadal summary maps was the spatial extent of areas with zero SWE values on April 1st for at least half the decade (5 years), within regions of CONUS with significant snow cover (***Figure 3***). These zero April 1st SWE areas are highlighted because they seem to contradict the convention in the western US that April 1st SWE represents total maximum seasonal snowpack accumulation (Bohr & Aguado, 2001; Musselman et al., 2019; Wrzesien et al., 2017). According to the UA SWE data, there was no snow cover on April 1st over various years in the 1980s, 1990s, 2000s, and 2010s, at the Portland Airport WBAN station (Maine, elevation: 14 m asl); the Buffalo Niagara Airport WBAN (New York, elev: 211m); the Minneapolis St. Paul Airport WBAN (Minnesota, elev: 255m); as well as at the Quemazon SNOTEL site (New Mexico, elev: 2898m); the Spratt Creek SNOTEL (California, elev: 1848m); and at the Cougar Mountain SNOTEL (Washington, elev: 975m) (***Figure 3***). For the six in-situ weather stations, the UA SWE data indicated one to four years of zero April 1st snow cover per decade at each station; totaling 18 data points in the 1980s, 19 in the 1990s, 23 in the 2000s, 22 in the 2010s, and an overall total of 82 modeled data points (***Figure 3***). On the ground "spot checks" at each station for each year resulted in a 93% agreement between observational and modeled data at the New England (Portland, ME) station, 100% agreement at the Northeast (Buffalo, NY) station, 94% in the Midwest at the Minneapolis, MN station, 73% at the Rocky Mountain (Quemazon, NM) SNOTEL site, 100% at the Spratt Creek SNOTEL in the Sierra Nevadas, CA, and only 31% at Pacific Northwest (Cougar Mountain, WA) SNOTEL (***Figure 3***).

In using the metric of zero April 1st SWE for the relatively small, sample group of 82 data points, as an evaluation tool for the UA SWE, we found agreement between the modeled data and the empirical data for 68 out of the 82 observations. This equates to an overall 83% agreement rate. Agreement rates at the SNOTEL sites across western CONUS were generally lower than those at the WBAN stations located in the Northeast and Midwest, with Cougar Mountain SNOTEL having the lowest agreement rate. When considering this sample of observational snow cover data, it is important to note that the SNOTEL sites in the western CONUS are often located in areas with preferential snow collecting capacity, as compared to the surrounding terrain. In

2021, a US Army Corps of Engineers report on Willow Creek in Idaho found that in extreme cases, some SNOTEL sites are located in tree islands with very poor representation of spatial average snow cover characteristics of the surrounding region (Giovando et al., 2021). This could account for more frequent snow cover on April 1st at the SNOTEL sites and lower agreements with the UA SWE data.

Similar to trends in maximum SWE values, our analysis of the UA data SCD indicates a decline in the number of snow days per pixel in each decadal average over the 40-year study period (***Figure 1b***), although the rate of decrease in number of snow covered days is less pronounced than the rate of decrease in maximum SWE values (***Figure 4a***). Average decadal maximum SWE and snow cover duration are also quantified and segmented by elevation band in ***Figure 4a.*** All decades and both metrics tend to increase proportional to elevation. For elevations under about 2,000m, all decades have similar values, comparatively, within each of the two snow cover metric datasets (***Figure 4a***). There is a value spread for both maximum SWE and SCD above the 2,000m elevation line, with the rate of spread generally increasing as elevation increases (***Figure 4a***). In 2018, Zeng et al. quantified and evaluated the UA SWE dataset and found that annual maximum SWE decreased by 41% on average for 13% of snowy pixels over the western US. They also found that annual SCD was shortened significantly by 34 days in 9% of the snowy pixels, with cool season (October through March) temperature and accumulated precipitation explaining the variability of 1st April SWE values over the western US and temperature alone as the primary influence on 1st April SWE in the eastern US (Zeng et al., 2018).

An alternative approach to showing the direct proportionality between SCD and elevation, is the evaluation of accumulation and ablation dates (***Figure 2, Figure 4b).*** These two season markers generally tend to spread further away from each other, temporally, with increase in elevation. Within each elevation band, SCD varies slightly from decade to decade, with the 1980s and 1990s generally being at least several days longer than the 2000s and 2010s above 2,000m elevation (***Figure 4b***). The increase in SCD by elevation appears to be weighted on the end of season ablation dates. In other words, start of accumulation dates at the highest elevation band (3,600m – 4,200m), for all decades, are roughly 55 days earlier than those at the lowest elevation band (0m – 400m) (***Figure 4b***). Meanwhile, end of ablation dates at the highest elevation occur more than 100 days later than those at the lowest elevation, with ablation dates tending to vary more per decade than accumulation dates, within a given elevation band (***Figure 4b***). Analogous to the line graph in ***Figure 4a***, the 30-year normal maximum SWE date shown in ***Figure 4b*** is relatively equal for each elevation band below 2,000m, and above that, maximum SWE increases with increase in elevation. Also, end of ablation dates are generally on or before April 1st below 2,000m and substantially later than that above this elevation (***Figure 4a***).

One reason why ablation dates tended to vary more per decade than accumulation dates could be related to annual changes in the diurnal cycle across CONUS. In our study area, accumulation begins relatively close to the winter solstice when hours of daylight are minimized. This results in low shortwave radiation inputs, when slight daily increases in average air temperature do not have a substantial impact on the snowpack (Garen & Marks, 2005). During this time of the year, small increases in sensible heat do not substantially impact the energy balance. Conversely, in the spring, daylight hours are increasing and a larger component of the energy balance equation consists of shortwave inputs. At this time, the snowpack is isothermal and small changes in sensible heat input can result in earlier and more rapid melt onset (Liston & Elder, 2006).

For both the maximum SWE and SCD, there are larger variations between decadal averages at higher elevations. The maximum spread between decadal traces is at approximately 4,000 m in elevation (***Figure 4a***). The DOWY start of accumulation varied more at lower elevations compared to the higher elevation bands. In contrast, the DOWY for the end of ablation was more variable between decades at the higher elevation bands (***Figure 4b***). A potential reason for this larger change between decades at higher elevations is that snow cover in these elevation bins tends to be seasonal, and therefore, the snowpack is subjected to longer ablation periods (Garen & Marks, 2005). Thus if late winter and early spring temperatures are changing, maximum accumulation could be impacted by climate change (with more precipitation occurring as rainfall). In contrast, lower elevation locations usually melt over a relatively compressed period earlier in the year and may not be impacted as much by increasing temperatures (Marks et al., 1999).

5.2 Snow Regime Classification System

The Snow Regime Classification system uses the gridded climate data (PRISM precipitation and UA SWE) to calculate ratios of SWE divided by cumulative cool season (October through March) precipitation using the dual approach of April 1st and maximum SWE. When the two ratios are thresholded into discrete classes, the results across CONUS are fairly different (***Figures 5*** and ***6***). Generally, the most southern regions of CONUS have class agreement as RD (*SWE / precipitation ratio < 0.1*) between the two ratio techniques. The Cascade, Rocky, and Sierra Nevada mountain ranges in Western CONUS also generally have the same classification, SD (*0.4 < SWE / precipitation ratio < 1.0*), with either ratio. However, the spatial extents of the snow regime classifications across these mountain ranges, when comparing the use of April 1st vs. maximum SWE, vary significantly (***Figures 5*** and ***6***).

While the spatial variability within the actual classifications between the two ratio approaches is substantial, that of the classification anomalies appears to be in somewhat better agreement. Both the April 1st and maximum SWE generated classes tend to have more solid precipitation than their respective 30-year normals in the mountain west of CONUS in the 1980's, as well as a swath of more liquid precipitation than the normal in the middle northern CONUS Dakotas region during the 1980s, 1990s, and 2000s (***Figure 7***). That same region also moves back towards more solid precipitation than the 30-year normal for both ratio methods in the 2010s (***Figure 7***). However, using the maximum SWE approach yields an additional set of anomalies that can be seen as a band of mixed solid and liquid precipitation phase shifts, which stretch across mid-west CONUS and are not evident with the April 1st SWE approach (***Figure 7***). Overall, the results of the Snow Regime Classification system indicate that previously SD areas have shifted to the R/S classification over the 40-year study period, with boundary lines moving up in latitude. These results are supported by previous studies that also found snow dominated regimes across CONUS to be declining (Barnett et al., 2005, 2008; Knowles et al., 2006; Mantua et al., 2010).

Our results are consistent with several key findings of the Fourth National Climate Assessment (NCA4): that Northern Hemisphere spring snow cover extent, North America maximum snow depth, SWE in the western US, and extreme snowfall years in the southern and western US have all declined, while extreme snowfall years in parts of the northern US have increased (USGCRP, 2017). Projections indicate large declines in snowpack in the western US and shifts to more precipitation falling as rain than snow in the cold season in many parts of the central and eastern US (USGCRP, 2017). These declines in snowpack extent, depth, and SWE are likely due to warming air temperatures that have been observed across CONUS for at least the last

60 years. The frequency of heat waves has increased since the mid-1960s, with the number of high temperature records set in the past two decades far exceeding the number of low temperature records (USGCRP, 2017).

5.3 SWE Input Data Comparison

In order to compare the two ratio thresholding approaches for generating the Snow Regime Classifications across CONUS, the quantitative evaluation includes a coverage area comparison of the RD, R/S, and SD classifications (***Figure 8***), a PRISM temperature analysis (***Figure 9***), and a comparison of the ratio calculation results per 200m elevation band in HUC2 regions across CONUS (***Figure 10***). Percent departures in classification areas from their respective 30-year normals show a decrease in SD regimes for both ratio methods during the 1980s, 1990s, and 2000s, with an increase following in the 2010s (***Figure 8***). RD areas displayed an analogous and opposite trend across the same time periods, i.e., increased for the first three decades, then decreased over the latest (***Figure 8***). For the transitional R/S regions with both ratio methods, percent departures in area decreased between the 1980's and 1990s, but generally increased during the remainder of the study period (***Figure 8***). The April 1st SWE and maximum SWE methods show similar decadal anomalies for RD, but frequently differ in both direction and percentage for R/S and SD areas (***Figure 8***). Areas across CONUS that have experienced increases in R/S regimes since the early 2000s are at particular risk for RoS flooding because snow cover in transitional regions is frequently at or near freezing. When liquid precipitation reaches an isothermal snowpack, it requires less energy for phase change and the snowpack easily melts, adding to runoff (Marks et al., 1998; Mazurkiewicz et al., 2008; Würzer et al., 2016). Additionally, because R/S regimes have warmer winters, RoS events are more likely, as cool season precipitation has a higher chance of falling as rain instead of snow (López-Moreno et al., 2021).

These trends for the anomalies in both the classification areal extents (***Figure 8***), as well as in the class precipitation phase shifts (***Figure 7***), may be explained, at least in part, by changes in air temperatures across CONUS during the study time period (***Figure 9***). The annual and cool season average air temperatures indicate more anomalous shifts towards the cold in the 1980's and 1990's (***Figure 9***), which appears to manifest in more solid precipitation during those decades (***Figures 7*** and ***8***). However, by the 2010s, air temperature anomalies indicate warmer annual averages, as well as strikingly warmer winters (cool seasons) (***Figure 9***). Yet the snow classifications show a shift back to colder regimes during this same time period in the 2010s (***Figures 7*** and ***8***). While the 2010s may have had the warmest winter anomalies (> 0.9° C), this decade also had the same number of coldest winter season anomalies as in the 1980s and 2000s (***Figure 9***). Over the 40 year study period, annual average air temperatures diverged from the 30-year normal the most in the 2010s, indicating a potential for greater variability in winter season temperatures during this decade (***Figure 9***).

In the comparison of the numerical results of the ratio calculations, using either of the two approaches, it can be seen that ratio values mostly increase at higher elevations, except for the HUC2-05 Ohio Region. At the very highest elevation bands, the ratio values slightly decrease in HUC2-01 New England, HUC2-07 Upper Mississippi, HUC2-16 Great Basin, HUC2-18 California, and for April 1st SWE ratios only in HUC2-10 Missouri and HUC2-11 Arkansas-White-Red (***Figure 10***). The graphical analysis of the ratio calculations, assembled and averaged by HUC02 WBD and by 200m elevation bands, show that the maximum SWE approach consistently yields larger values than the April 1st SWE approach (***Figure 10***). However, the values

from both ratio techniques vary by elevation band with similar patterns. Only the HUC2-06 Tennessee region appears to have ratio values that do not vary correspondingly between the two approaches (***Figure 10***).

Changes in Snow Regimes in arid and semi-arid regions where snow is critical for municipal and/or agricultural water supply are becoming increasingly salient across western CONUS (P. W. Mote et al., 2018; Pederson et al., 2013). Some of these regions include the HUC2-13 Rio Grande, HUC2-14 Upper Colorado, HUC2-15 Lower Colorado, and HUC2-16 Great Basin regions (***Figures 10c, 10d***). Trends in ratio values for these areas appear to show slight decreases in values at comparable elevations over the decades across the study period. Another way to frame this is that the same ratio values are moving up slightly in elevation over time (***Figures 10c, 10d***). This could mean a decrease in SD areas and an increase in R/S and RD areas. If less of the overall water budget in these regions is being stored as snowpack, this could shift the timing of peak runoff to earlier in the water year, as well as decreasing the magnitude of the peak, with more moisture arriving in the watershed via warm season rains and less as spring snowmelt. Such changes could impact water resource management in these areas of the arid west.

In flood prone areas of CONUS, such as the HUC2-07 Upper Mississippi Region, decadal changes in ratio values by elevation indicate a general trend toward higher ratio values above 500 meters over time (***Figure 10b***). This trend is most consistent over the decades for the April 1st SWE ratio approach in the Upper Mississippi, although there is also an abrupt change in this direction between the 2000s and 2010s for the maximum SWE ratio technique (***Figure 10b***). In this HUC2, ratios indicate that the region is generally classified as transitional (R/S), with ratio values above 500m occurring on the lower side of the R/S range. As ratio values above this elevation start to increase over the decades, they are approaching the SD classification. Such temporal changes could shift the timing and magnitude of runoff in this region, and increase potential rain-on-snow flooding from extreme rainfall events occurring over a thin, temperate snowpack (Musselman et al., 2018). Such events may be influenced by climactic changes dependent on topographic variables occurring over time (López-Moreno et al., 2021; McCabe et al., 2007), such as is seen in the ratio values in the Upper Mississippi (***Figure 10b***).

Some areas where there is a substantial divergence between the results from the April 1st and maximum SWE ratio approaches include the HUC2-02 Mid-Atlantic, HUC2-05 Ohio, and HUC2-06 Tennessee regions (***Figures 10a, 10b***). These eastern regions of CONUS have a lower range of elevations (0m to 1600m) as compared those in the west (0m to about 4,000m). The Mid-Atlantic, Ohio, and Tennessee regions display a larger difference in ratio values between the two techniques, however this is only relative, as the range of ratios is smaller across a less variable elevation range. Overall, differences in ratios are roughly 0.2, which is similar to regions in western CONUS (***Figures 10c, 10d***).

Decreases in the ratio values for both approaches are evident at higher elevations for the HUC2-01 New England, HUC2-05 Ohio, HUC2-07 Upper Mississippi, and HUC2-15 Lower Colorado regions (***Figure 10***). Additionally, in these regions for the 2010s, ratio values at these elevations tend to diverge from each other more. One contributing factor to inconsistencies in these trends at higher elevations could be an implicit data scarcity issue, as there are fewer weather stations at these elevations across CONUS and therefore less observational data were available to calibrate both the PRISM and UA models. For example, in HUC2-15 Lower Colorado Region, the

highest elevations are at the southern end of the watershed, which might explain the double-back pattern in the lines (***Figure 10d***).

Overall, anomalies in snow dominated extent, compared to the 30-year normal, decreased in the 1980s, 1990s, and 2000s, while those of rain dominated increased. Such decadal climatic shifts and changes in snow hydrologic regimes for CONUS over the last 40 years have been observed in other studies (Musselman et al., 2018). The connection between changes in the snow regime classifications over the 40-year study period are likely partly dependent on climate-driven changes in air temperatures (McCabe et al., 2007), which influence snowpack behavior like timing of melt and persistence (Heggli et al., 2022; Marks et al., 1998, 1999; Singh et al., 1997).

6 Conclusions

As the climate continues to change, regions across CONUS are experiencing rapid snow regime shifts that test the design limits of water resource infrastructure. Communities and economies dependent on this infrastructure are becoming more and more at risk of negative impacts from extreme hydrologic events due to changing snowmelt patterns. Therefore, this study uses a new geo-spatial snow regime classification system, based on the ratio of maximum SWE to cool season precipitation, to track climate driven changes in snow hydrology across CONUS over 40 years (1981 – 2020). The snow regime classes include: (1) rain dominated (RD), (2) snow dominated (SD), (3) transitional (R/S), or (4) perennial snow (PS).

Results indicate that average snow cover duration generally became shorter in each decade over the 40-year period, with the rate of decline increasing with elevation. Anomalies in SD extents, compared to the 30-year normal (1991 – 2020), decreased in the 1980s, 1990s, and 2000s, while anomalies of RD extents increased. Also, previously SD areas have shifted to the transitional classification (R/S) over the 40-year study period, with boundary lines moving up in latitude. As CONUS water and land managers and government agencies find the need to adapt to a changing climate, geospatial classification, such as our snow regime approach, could be a critical tool.

Acknowledgments

The authors declare no real or perceived financial conflicts of interest, nor any affiliations that may be perceived as having a conflict of interest with the results of this paper.

This work was funded by the US Army Engineer Research and Development Center through the Flood and Coastal Systems Research and Development Program's Enhanced Snowmelt Modeling work unit and the Post-Wildfire Research and Development Program's Rain-on-Snow work unit.

This research was also supported in part by an appointment to the Department of Defense (DOD) Research Participation Program administered by the Oak Ridge Institute for Science and Education (ORISE) through an interagency agreement between the U.S. Department of Energy (DOE) and the DOD. ORISE is managed by ORAU under DOE contract number DE-SC0014664. All opinions expressed in this paper are the author's and do not necessarily reflect the policies and views of DOD, DOE, or ORAU/ORISE.

The authors would like to thank the Oak Ridge Institute for Science and Education's (ORISE) Postdoctoral Research Fellowship program for facilitating support for Dr. Tedesche. We would also like to thank Ms. Jane Harrell at the US Army Corps of Engineers, Seattle District, for her contribution related to preliminary computational idea development of this research.

Open Research

Research Product Availability:

To provide the results of this study as a useable geospatial tool, the Snow Regime Classifications are available as annual maps, spanning the full spatial extent of CONUS, for water years 1982 through 2020 (1 October through 30 September). These maps are available for download as GeoTIFF files at the 4 km grid scale at: http://dx.doi.org/10.21079/11681/46021

Supporting Information Availability:

A flow chart of study methods, animated CONUS maps of annual snow cover metrics related to the UA SWE dataset evaluation, and animations of annual Snow Regime Classifications (presented as decadal averages in the primary document) are available as ***Figure S1*** and ***Data Sets S1 through S8,*** respectively, in ***Supporting Information for Changing Snow Regime Classifications across the Contiguous United States***.

Data Availability:

The Daily 4 km Gridded SWE and Snow Depth from Assimilated In-Situ and Modeled Data over the Conterminous US, Version 1 are available at:
https://nsidc.org/data/nsidc-0719/versions/1

For processing via Google Earth Engine (GEE), the PRISM Daily Spatial Climate Dataset:
https://developers.google.com/earth-engine/datasets/catalog/OREGONSTATE_PRISM_AN81d

Also available in GEE are the HUC02: USGS Watershed Boundary Dataset of Regions:
https://developers.google.com/earth-engine/datasets/catalog/USGS_WBD_2017_HUC02

The USGS 3DEP 10m National Map Seamless (1/3 Arc-Second) digital elevation model (DEM):
https://developers.google.com/earth-engine/datasets/catalog/USGS_3DEP_10m

Code Availability:

Codes for the evaluation of the UA SWE dataset and for generating and evaluating the Snow Regime Classifications for CONUS are available at:
https://code.earthengine.google.com/df163f030c96e4f30ae5c7ff0adc85f8
https://code.earthengine.google.com/0a88d50e3135433bfbdf2d05567ef2ab

Codes for visualizing the results of this study is available at:
https://code.earthengine.google.com/bd9097f4320850423c76a2ce1681e6d2
https://code.earthengine.google.com/922c938c725f649581f65046b22c5d72
https://code.earthengine.google.com/d9dece9ef9016953d1bd680376009177

References

Abatzoglou, J. T. (2011). Influence of the PNA on declining mountain snowpack in the Western United States. *International Journal of Climatology*, *31*(8), 1135–1142. https://doi.org/10.1002/joc.2137

Barnett, T. P., Adam, J. C., & Lettenmaier, D. P. (2005). Potential impacts of a warming climate on water availability in snow-dominated regions. *Nature*, *438*(7066), 303–309. https://doi.org/10.1038/nature04141

Barnett, T. P., Pierce, D. W., Hidalgo, H. G., Bonfils, C., Santer, B. D., Das, T., Bala, G., Wood, A. W., Nozawa, T., Mirin, A. A., Cayan, D. R., & Dettinger, M. D. (2008). Human-Induced Changes in the Hydrology of the Western United States. *Science*, *319*(5866), 1080–1083. https://doi.org/10.1126/science.1152538

Bohr, G. S., & Aguado, E. (2001). Use of April 1 SWE measurements as estimates of peak seasonal snowpack and total cold-season precipitation. *Water Resources Research*, *37*(1), 51–60. https://doi.org/10.1029/2000WR900256

Brown, R. D. (2000). Northern Hemisphere Snow Cover Variability and Change, 1915–97. *Journal of Climate*, *13*(13), 2339–2355. https://doi.org/10.1175/1520-0442(2000)013<2339:NHSCVA>2.0.CO;2

Broxton, P. D., Dawson, N., & Zeng, X. (2016). Linking snowfall and snow accumulation to generate spatial maps of SWE and snow depth. *Earth and Space Science*, *3*(6), 246–256. https://doi.org/10.1002/2016EA000174

Burton, H. K. (1916). SNOW SURVEYS IN BIG COTTONWOOD CANYON, UTAH, 1912 TO 1916. *Monthly Weather Review*, *44*(6), 360–361. https://doi.org/10.1175/1520-0493(1916)44<360:SSIBCC>2.0.CO;2

882 Cayan, D. R. (1996). Interannual Climate Variability and Snowpack in the Western United
883 States. *Journal of Climate*, *9*(5), 928–948. https://doi.org/10.1175/1520-
884 0442(1996)009<0928:ICVASI>2.0.CO;2
885 Curran, J. H., & Biles, F. E. (2021). Identification of Seasonal Streamflow Regimes and
886 Streamflow Drivers for Daily and Peak Flows in Alaska. *Water Resources Research*,
887 *57*(2). https://doi.org/10.1029/2020WR028425
888 Daly, C., Dogget, M. K., Smith, J. I., Olson, K. V., Halbleib, M. D., Dimcovic, Z., Keon, D.,
889 Loiselle, R. A., Steinberg, B., Ryan, A. D., Pancake, C. M., & Kaspar, E. M. (2021).
890 Challenges in Observation-Based Mapping of Daily Precipitation across the
891 Conterminous United States. *Journal of Atmospheric and Oceanic Technology*, *38*(11),
892 1979–1992. https://doi.org/10.1175/JTECH-D-21-0054.1
893 Daly, C., Halbleib, M., Smith, J. I., Gibson, W. P., Doggett, M. K., Taylor, G. H., Curtis, J., &
894 Pasteris, P. P. (2008). Physiographically sensitive mapping of climatological temperature
895 and precipitation across the conterminous United States. *International Journal of*
896 *Climatology*, *28*(15), 2031–2064. https://doi.org/10.1002/joc.1688
897 Daly, C., Slater, M. E., Roberti, J. A., Laseter, S. H., & Swift, L. W. (2017). High-resolution
898 precipitation mapping in a mountainous watershed: Ground truth for evaluating
899 uncertainty in a national precipitation dataset. *International Journal of Climatology*, *37*,
900 124–137. https://doi.org/10.1002/joc.4986
901 Dawson, N., Broxton, P., & Zeng, X. (2018). Evaluation of Remotely Sensed Snow Water
902 Equivalent and Snow Cover Extent over the Contiguous United States. *Journal of*
903 *Hydrometeorology*, *19*(11), 1777–1791. https://doi.org/10.1175/JHM-D-18-0007.1

Dolant, C., Langlois, A., Montpetit, B., Brucker, L., Roy, A., & Royer, A. (2016). Development of a rain-on-snow detection algorithm using passive microwave radiometry. *Hydrological Processes*, *30*(18), 3184–3196. https://doi.org/10.1002/hyp.10828

Elsner, M. M., Cuo, L., Voisin, N., Deems, J. S., Hamlet, A. F., Vano, J. A., Mickelson, K. E. B., Lee, S.-Y., & Lettenmaier, D. P. (2010). Implications of 21st century climate change for the hydrology of Washington State. *Climatic Change*, *102*(1–2), 225–260. https://doi.org/10.1007/s10584-010-9855-0

Fassnacht, S. R., Cherry, M. L., Venable, N. B. H., & Saavedra, F. (2016). Snow and albedo climate change impacts across the United States Northern Great Plains. *The Cryosphere*, *10*(1), 329–339. https://doi.org/10.5194/tc-10-329-2016

Fisher, L. C. (1918). SNOWFALL ON MOUNT RANIER, WASH. *Monthly Weather Review*, *46*(7), 327–330. https://doi.org/10.1175/1520-0493(1918)46<327:SOMRW>2.0.CO;2

Garen, D. C., & Marks, D. (2005). Spatially distributed energy balance snowmelt modelling in a mountainous river basin: Estimation of meteorological inputs and verification of model results. *Journal of Hydrology*, *315*(1–4), 126–153. https://doi.org/10.1016/j.jhydrol.2005.03.026

Giovando, J., Engel, C., Daly, S., Warner, M., Hamill, D., & Heisman, E. (2021). *Wintertime snow and precipitation conditions in the Willow Creek watershed above Ririe Dam, Idaho*. Engineer Research and Development Center (U.S.). https://doi.org/10.21079/11681/40479

Giovando, J., & Niemann, J. D. (2022). Wildfire Impacts on Snowpack Phenology in a Changing Climate Within the Western U.S. *Water Resources Research*, *58*(8). https://doi.org/10.1029/2021WR031569

927 Gorelick, N., Hancher, M., Dixon, M., Ilyushchenko, S., Thau, D., & Moore, R. (2017). Google
928 Earth Engine: Planetary-scale geospatial analysis for everyone. *Remote Sensing of*
929 *Environment*, *202*, 18–27.
930 Goss, M., Swain, D. L., Abatzoglou, J. T., Sarhadi, A., Kolden, C. A., Williams, A. P., &
931 Diffenbaugh, N. S. (2020). Climate change is increasing the likelihood of extreme
932 autumn wildfire conditions across California. *Environmental Research Letters*, *15*(9),
933 094016. https://doi.org/10.1088/1748-9326/ab83a7
934 Grenfell, T. C., & Putkonen, J. (2008). A method for the detection of the severe rain-on-snow
935 event on Banks Island, October 2003, using passive microwave remote sensing. *Water*
936 *Resources Research*, *44*(3). https://doi.org/10.1029/2007WR005929
937 Groisman, P. Y., Knight, R. W., Karl, T. R., Easterling, D. R., Sun, B., & Lawrimore, J. H.
938 (2004). Contemporary Changes of the Hydrological Cycle over the Contiguous United
939 States: Trends Derived from In Situ Observations. *Journal of Hydrometeorology*, *5*(1),
940 64–85. https://doi.org/10.1175/1525-7541(2004)005<0064:CCOTHC>2.0.CO;2
941 Hamill, D., Giovando, J., Engel, C., Dahl, T., & Bartles, M. (2021). *Application of a Radiation-*
942 *Derived Temperature Index Model to the Willow Creek Watershed in Idaho, USA*.
943 ENGINEER RESEARCH AND DEVELOPMENT CENTER HANOVER NH.
944 https://apps.dtic.mil/sti/citations/AD1144235
945 Hamlet, A. F., & Lettenmaier, D. P. (2007). Effects of 20th century warming and climate
946 variability on flood risk in the western U.S.: EFFECTS OF 20TH CENTURY
947 WARMING ON FLOOD. *Water Resources Research*, *43*(6).
948 https://doi.org/10.1029/2006WR005099

949 Hammond, J. C., Saavedra, F. A., & Kampf, S. K. (2018). Global snow zone maps and trends in
950 snow persistence 2001–2016. *International Journal of Climatology*, *38*(12), 4369–4383.
951 https://doi.org/10.1002/joc.5674
952 Harrison, H. N., Hammond, J. C., Kampf, S., & Kiewiet, L. (2021). On the hydrological
953 difference between catchments above and below the intermittent-persistent snow
954 transition. *Hydrological Processes*, *35*(11). https://doi.org/10.1002/hyp.14411
955 Heggli, A., Hatchett, B., Schwartz, A., Bardsley, T., & Hand, E. (2022). Toward snowpack
956 runoff decision support. *IScience*, *25*(5), 104240.
957 https://doi.org/10.1016/j.isci.2022.104240
958 Jefferson, A. J. (2011). Seasonal versus transient snow and the elevation dependence of climate
959 sensitivity in maritime mountainous regions. *Geophysical Research Letters*, *38*(16), 1–7.
960 https://doi.org/10.1029/2011GL048346
961 Kampf, S. K., & Lefsky, M. A. (2016). Transition of dominant peak flow source from snowmelt
962 to rainfall along the Colorado Front Range: Historical patterns, trends, and lessons from
963 the 2013 Colorado Front Range floods. *Water Resources Research*, *52*(1), 407–422.
964 https://doi.org/10.1002/2015WR017784
965 Kampf, S. K., & Richer, E. E. (2014). Estimating source regions for snowmelt runoff in a Rocky
966 Mountain basin: Tests of a data-based conceptual modeling approach. *Hydrological*
967 *Processes*, *28*(4), 2237–2250. https://doi.org/10.1002/hyp.9751
968 Klos, P. Z., Link, T. E., & Abatzoglou, J. T. (2014). Extent of the rain-snow transition zone in
969 the western U.S. under historic and projected climate. *Geophysical Research Letters*,
970 *41*(13), 4560–4568. https://doi.org/10.1002/2014GL060500

971 Kluver, D., & Leathers, D. (2015). Regionalization of snowfall frequency and trends over the
972 contiguous United States. *International Journal of Climatology*, *35*(14), 4348–4358.
973 https://doi.org/10.1002/joc.4292
974 Knowles, N. (2015). Trends in Snow Cover and Related Quantities at Weather Stations in the
975 Conterminous United States. *Journal of Climate*, *28*(19), 7518–7528.
976 https://doi.org/10.1175/JCLI-D-15-0051.1
977 Knowles, N., Dettinger, M. D., & Cayan, D. R. (2006). Trends in Snowfall versus Rainfall in the
978 Western United States. *Journal of Climate*, *19*(18), 4545–4559.
979 https://doi.org/10.1175/JCLI3850.1
980 Kunkel, K. E., Palecki, M., Ensor, L., Hubbard, K. G., Robinson, D., Redmond, K., & Easterling,
981 D. (2009). Trends in Twentieth-Century U.S. Snowfall Using a Quality-Controlled
982 Dataset. *Journal of Atmospheric and Oceanic Technology*, *26*(1), 33–44.
983 https://doi.org/10.1175/2008JTECHA1138.1
984 Kunkel, K. E., Robinson, D. A., Champion, S., Yin, X., Estilow, T., & Frankson, R. M. (2016).
985 Trends and Extremes in Northern Hemisphere Snow Characteristics. *Current Climate*
986 *Change Reports*, *2*(2), 65–73. https://doi.org/10.1007/s40641-016-0036-8
987 Lader, R., Walsh, J. E., Bhatt, U. S., & Bieniek, P. A. (2020). Anticipated changes to the snow
988 season in Alaska: Elevation dependency, timing and extremes. *International Journal of*
989 *Climatology*, *40*(1), 169–187. https://doi.org/10.1002/joc.6201
990 Li, D., Lettenmaier, D. P., Margulis, S. A., & Andreadis, K. (2019). The Role of Rain-on-Snow
991 in Flooding Over the Conterminous United States. *Water Resources Research*, *55*(11),
992 8492–8513. https://doi.org/10.1029/2019WR024950

993 Liston, G. E., & Elder, K. (2006). A Distributed Snow-Evolution Modeling System
994 (SnowModel). *Journal of Hydrometeorology*, *7*(6), 1259–1276.
995 https://doi.org/10.1175/JHM548.1
996 López-Moreno, J. I., Pomeroy, J. W., Morán-Tejeda, E., Revuelto, J., Navarro-Serrano, F. M.,
997 Vidaller, I., & Alonso-González, E. (2021). Changes in the frequency of global high
998 mountain rain-on-snow events due to climate warming. *Environmental Research Letters*,
999 *16*(9), 094021. https://doi.org/10.1088/1748-9326/ac0dde
1000 Mantua, N., Tohver, I., & Hamlet, A. (2010). Climate change impacts on streamflow extremes
1001 and summertime stream temperature and their possible consequences for freshwater
1002 salmon habitat in Washington State. *Climatic Change*, *102*(1–2), 187–223.
1003 https://doi.org/10.1007/s10584-010-9845-2
1004 Marks, D., Domingo, J., Susong, D., Link, T., & Garen, D. (1999). A spatially distributed energy
1005 balance snowmelt model for application in mountain basins. *Hydrological Processes*,
1006 *13*(12–13), 1935–1959. https://doi.org/10.1002/(SICI)1099-
1007 1085(199909)13:12/13<1935::AID-HYP868>3.0.CO;2-C
1008 Marks, D., Kimball, J., Tingey, D., & Link, T. (1998). The sensitivity of snowmelt processes to
1009 climate conditions and forest cover during rain-on-snow: A case study of the 1996 Pacific
1010 Northwest flood. *Hydrological Processes*, *12*(10–11), 1569–1587.
1011 https://doi.org/10.1002/(SICI)1099-1085(199808/09)12:10/11<1569::AID-
1012 HYP682>3.0.CO;2-L
1013 Marks, D., Link, T., Winstral, A., & Garen, D. (2001). Simulating snowmelt processes during
1014 rain-on-snow over a semi-arid mountain basin. *Annals of Glaciology*, *32*, 195–202.
1015 https://doi.org/10.3189/172756401781819751

1016 Marks, D., Winstral, A., Reba, M., Pomeroy, J., & Kumar, M. (2013). An evaluation of methods
1017 for determining during-storm precipitation phase and the rain/snow transition elevation at
1018 the surface in a mountain basin. *Advances in Water Resources*, *55*, 98–110.
1019 https://doi.org/10.1016/j.advwatres.2012.11.012
1020 Mazurkiewicz, A. B., Callery, D. G., & McDonnell, J. J. (2008). Assessing the controls of the
1021 snow energy balance and water available for runoff in a rain-on-snow environment.
1022 *Journal of Hydrology*, *354*(1–4), 1–14. https://doi.org/10.1016/j.jhydrol.2007.12.027
1023 McCabe, G. J., Clark, M. P., & Hay, L. E. (2007). Rain-on-Snow Events in the Western United
1024 States. *Bulletin of the American Meteorological Society*, *88*(3), 319–328.
1025 https://doi.org/10.1175/BAMS-88-3-319
1026 Moore, C., Kampf, S., Stone, B., & Richer, E. (2015). A GIS-based method for defining snow
1027 zones: Application to the western United States. *Geocarto International*, *30*(1), 62–81.
1028 https://doi.org/10.1080/10106049.2014.885089
1029 Mote, P., Hamlet, A., & Salathé, E. (2008). Has spring snowpack declined in the Washington
1030 Cascades? *Hydrology and Earth System Sciences*, *12*(1), 193–206.
1031 https://doi.org/10.5194/hess-12-193-2008
1032 Mote, P. W., Hamlet, A. F., Clark, M. P., & Lettenmaier, D. P. (2005). DECLINING
1033 MOUNTAIN SNOWPACK IN WESTERN NORTH AMERICA*. *Bulletin of the*
1034 *American Meteorological Society*, *86*(1), 39–50. https://doi.org/10.1175/BAMS-86-1-39
1035 Mote, P. W., Li, S., Lettenmaier, D. P., Xiao, M., & Engel, R. (2018). Dramatic declines in
1036 snowpack in the western US. *Npj Climate and Atmospheric Science*, *1*(1), Article 1.
1037 https://doi.org/10.1038/s41612-018-0012-1

1038 Musselman, K. N., Addor, N., Vano, J., & Molotch, N. P. (2019). RECONSIDERING THE
1039 UTILITY OF THE APRIL 1ST SNOW WATER EQUIVALENT METRIC FOR
1040 WATER RESOURCE APPLICATIONS. *Western Snow Conference*, 4.
1041 Musselman, K. N., Lehner, F., Ikeda, K., Clark, M. P., Prein, A. F., Liu, C., Barlage, M., &
1042 Rasmussen, R. (2018). Projected increases and shifts in rain-on-snow flood risk over
1043 western North America. *Nature Climate Change*, *8*(9), 808–812.
1044 https://doi.org/10.1038/s41558-018-0236-4
1045 NOAA, (National Oceanic and Atmospheric Administration). (2019). Federal Meteorological
1046 Handbook No. 1: Surface Weather Observations and Reports. FCM-H1-2019.
1047 *Washington, DC: Office of the Federal Coordinator for Meteorological Services and*
1048 *Supporting Research*, 101.
1049 Nolin, A. W., & Daly, C. (2006). Mapping "At Risk" Snow in the Pacific Northwest. *Journal of*
1050 *Hydrometeorology*, *7*(5), 1164–1171. https://doi.org/10.1175/JHM543.1
1051 Nolin, A. W., Sproles, E. A., Rupp, D. E., Crumley, R. L., Webb, M. J., Palomaki, R. T., & Mar,
1052 E. (2021). New snow metrics for a warming world. *Hydrological Processes*, *35*(6).
1053 https://doi.org/10.1002/hyp.14262
1054 Ocampo Melgar, D., & Meza, F. J. (2020). Exploring the Fingerprints of Past Rain-on-Snow
1055 Events in a Central Andean Mountain Range Basin Using Satellite Imagery. *Remote*
1056 *Sensing*, *12*(24), 4173. https://doi.org/10.3390/rs12244173
1057 Pan, C. G., Kirchner, P. B., Kimball, J. S., Du, J., & Rawlins, M. A. (2021). Snow Phenology
1058 and Hydrologic Timing in the Yukon River Basin, AK, USA. *Remote Sensing*, *13*(12),
1059 2284. https://doi.org/10.3390/rs13122284

1060 Pan, C. G., Kirchner, P. B., Kimball, J. S., Kim, Y., & Du, J. (2018). Rain-on-snow events in
1061 Alaska, their frequency and distribution from satellite observations. *Environmental*
1062 *Research Letters*, *13*(7), 075004. https://doi.org/10.1088/1748-9326/aac9d3
1063 Pederson, G. T., Betancourt, J. L., & McCabe, G. J. (2013). Regional patterns and proximal
1064 causes of the recent snowpack decline in the Rocky Mountains, U.S. *Geophysical*
1065 *Research Letters*, *40*(9), 1811–1816. https://doi.org/10.1002/grl.50424
1066 Pradhanang, S. M., Frei, A., Zion, M., Schneiderman, E. M., Steenhuis, T. S., & Pierson, D.
1067 (2013). Rain-on-snow runoff events in New York. *Hydrological Processes*, *27*(21),
1068 3035–3049. https://doi.org/10.1002/hyp.9864
1069 Qi, J., Li, S., Jamieson, R., Hebb, D., Xing, Z., & Meng, F.-R. (2017). Modifying SWAT with an
1070 energy balance module to simulate snowmelt for maritime regions. *Environmental*
1071 *Modelling & Software*, *93*, 146–160. https://doi.org/10.1016/j.envsoft.2017.03.007
1072 Richer, E. E., Kampf, S. K., Fassnacht, S. R., & Moore, C. C. (2013). Spatiotemporal index for
1073 analyzing controls on snow climatology: Application in the Colorado Front Range.
1074 *Physical Geography*, *34*(2), 85–107. https://doi.org/10.1080/02723646.2013.787578
1075 Rücker, A., Boss, S., Kirchner, J. W., & von Freyberg, J. (2019). Monitoring snowpack outflow
1076 volumes and their isotopic composition to better understand streamflow generation
1077 during rain-on-snow events. *Hydrology and Earth System Sciences*, *23*(7), 2983–3005.
1078 https://doi.org/10.5194/hess-23-2983-2019
1079 Saavedra, F. A., Kampf, S. K., Fassnacht, S. R., & Sibold, J. S. (2017). A snow climatology of
1080 the Andes Mountains from MODIS snow cover data: A snow climatology of the Andes
1081 Mountains. *International Journal of Climatology*, *37*(3), 1526–1539.
1082 https://doi.org/10.1002/joc.4795

1083 Schnorbus, M., Werner, A., & Bennett, K. (2014). Impacts of climate change in three hydrologic
1084 regimes in British Columbia, Canada. *Hydrological Processes*, *28*(3), 1170–1189.
1085 https://doi.org/10.1002/hyp.9661
1086 Scott, D., Dawson, J., & Jones, B. (2008). Climate change vulnerability of the US Northeast
1087 winter recreation– tourism sector. *Mitigation and Adaptation Strategies for Global*
1088 *Change*, *13*(5–6), 577–596. https://doi.org/10.1007/s11027-007-9136-z
1089 Singh, P., Spitzbart, G., Hübl, H., & Weinmeister, H. W. (1997). Hydrological response of
1090 snowpack under rain-on-snow events: A field study. *Journal of Hydrology*, *202*(1–4), 1–
1091 20. https://doi.org/10.1016/S0022-1694(97)00004-8
1092 Stone, R. S., Dutton, E. G., Harris, J. M., & Longenecker, D. (2002). Earlier spring snowmelt in
1093 northern Alaska as an indicator of climate change. *Journal of Geophysical Research:*
1094 *Atmospheres*, *107*(D10), ACL 10-1-ACL 10-13. https://doi.org/10.1029/2000JD000286
1095 Strachan, S., & Daly, C. (2017). Testing the daily PRISM air temperature model on semiarid
1096 mountain slopes. *Journal of Geophysical Research: Atmospheres*, *122*(11), 5697–5715.
1097 https://doi.org/10.1002/2016JD025920
1098 Sturm, M., Holmgren, J., & Liston, G. E. (1995). A Seasonal Snow Cover Classification System
1099 for Local to Global Applications. *Journal of Climate*, *8*(5), 1261–1283.
1100 https://doi.org/10.1175/1520-0442(1995)008<1261:ASSCCS>2.0.CO;2
1101 Svoma, B. M. (2011). Trends in snow level elevation in the mountains of central Arizona.
1102 *International Journal of Climatology*, *31*(1), 87–94. https://doi.org/10.1002/joc.2062
1103 Takala, M., Luojus, K., Pulliainen, J., Derksen, C., Lemmetyinen, J., Kärnä, J.-P., Koskinen, J.,
1104 & Bojkov, B. (2011). Estimating northern hemisphere snow water equivalent for climate
1105 research through assimilation of space-borne radiometer data and ground-based

measurements. *Remote Sensing of Environment*, *115*(12), 3517–3529. https://doi.org/10.1016/j.rse.2011.08.014

Tohver, I. M., Hamlet, A. F., & Lee, S.-Y. (2014). Impacts of 21st-Century Climate Change on Hydrologic Extremes in the Pacific Northwest Region of North America. *JAWRA Journal of the American Water Resources Association*, *50*(6), 1461–1476. https://doi.org/10.1111/jawr.12199

Trujillo, E., & Molotch, N. P. (2014). Snowpack regimes of the Western United States. *Water Resources Research*, *50*(7), 5611–5623. https://doi.org/10.1002/2013WR014753

USGCRP. (2017). *Climate Science Special Report: Fourth National Climate Assessment, Volume I [Wuebbles, D.J., D.W. Fahey, K.A. Hibbard, D.J. Dokken, B.C. Stewart, and T.K. Maycock (eds.)]* (p. 470). US Global Change Research Program, Washington, DC, USA.

Vano, J. A., Nijssen, B., & Lettenmaier, D. P. (2015). Seasonal hydrologic responses to climate change in the Pacific Northwest. *Water Resources Research*, *51*(4), 1959–1976. https://doi.org/10.1002/2014WR015909

Vormoor, K., Lawrence, D., Heistermann, M., & Bronstert, A. (2015). Climate change impacts on the seasonality and generation processes of floods – projections and uncertainties for catchments with mixed snowmelt/rainfall regimes. *Hydrology and Earth System Sciences*, *19*(2), 913–931. https://doi.org/10.5194/hess-19-913-2015

Wachowicz, L. J., Mote, T. L., & Henderson, G. R. (2020). A rain on snow climatology and temporal analysis for the eastern United States. *Physical Geography*, *41*(1), 54–69. https://doi.org/10.1080/02723646.2019.1629796

1128 Wayand, N. E., Lundquist, J. D., & Clark, M. P. (2015). Modeling the influence of hypsometry,
1129 vegetation, and storm energy on snowmelt contributions to basins during rain-on-snow
1130 floods. *Water Resources Research*, *51*(10), 8551–8569.
1131 https://doi.org/10.1002/2014WR016576
1132 Wever, N., Jonas, T., Fierz, C., & Lehning, M. (2014). Model simulations of the modulating
1133 effect of the snow cover in a rain-on-snow event. *Hydrology and Earth System Sciences*,
1134 *18*(11), 4657–4669. https://doi.org/10.5194/hess-18-4657-2014
1135 Wrzesien, M. L., Durand, M. T., Pavelsky, T. M., Howat, I. M., Margulis, S. A., & Huning, L. S.
1136 (2017). Comparison of Methods to Estimate Snow Water Equivalent at the Mountain
1137 Range Scale: A Case Study of the California Sierra Nevada. *Journal of*
1138 *Hydrometeorology*, *18*(4), 1101–1119. https://doi.org/10.1175/JHM-D-16-0246.1
1139 Würzer, S., Jonas, T., Wever, N., & Lehning, M. (2016). Influence of Initial Snowpack
1140 Properties on Runoff Formation during Rain-on-Snow Events. *Journal of*
1141 *Hydrometeorology*, *17*(6), 1801–1815. https://doi.org/10.1175/JHM-D-15-0181.1
1142 Würzer, S., Wever, N., Juras, R., Lehning, M., & Jonas, T. (2017). Modelling liquid water
1143 transport in snow under rain-on-snow conditions – considering preferential flow.
1144 *Hydrology and Earth System Sciences*, *21*(3), 1741–1756. https://doi.org/10.5194/hess-
1145 21-1741-2017
1146 Zeng, X., Broxton, P., & Dawson, N. (2018). Snowpack Change From 1982 to 2016 Over
1147 Conterminous United States. *Geophysical Research Letters*, *45*(23).
1148 https://doi.org/10.1029/2018GL079621
1149
1150